Corrosion Science 205 (2022) 110443

Contents lists available at ScienceDirect

Corrosion Science

journal homepage: www.elsevier.com/locate/corsci

How adsorbed H, O, OH, and Cl affect plain adsorption of imidazole on copper

Matjaž Dlouhy [a,b,1], Anton Kokalj [a,b,*,2]

[a] Department of Physical and Organic Chemistry, Jožef Stefan Institute, Jamova 39, SI-1000 Ljubljana, Slovenia
[b] Jožef Stefan International Postgraduate School, Jamova 39, SI-1000 Ljubljana, Slovenia

ARTICLE INFO

Keywords:
Density-functional theory calculations
Coadsorption
Lateral interactions
Azoles
Corrosion inhibitors
Work function

ABSTRACT

In real environments, metal surfaces are never clean. Even during active dissolution in corrosion, they are likely covered with adsorbed species such as O, OH, H, and Cl. For this reason, we addressed how such species (hereinafter labeled as $X_{(ads)}$) affect the adsorption bonding of imidazole—used as an archetypal model of azole corrosion inhibitors—on Cu(111). To this end, we performed a systematic high-throughput DFT study by considering over 400 different adsorption configurations, where the effects of coverage, the type of $X_{(ads)}$ species, and the distance between imidazole and $X_{(ads)}$ were scrutinized. Our calculations indicate that O and Cl enhance the adsorption bonding of imidazole, H has almost no effect, whereas OH either diminishes or has a negligible impact on the adsorption of imidazole. The effect of the $X_{(ads)}$ species on the imidazole adsorption usually diminishes with the increasing distance between $X_{(ads)}$ and imidazole and with decreasing $X_{(ads)}$ coverage. Three coadsorption effects of $X_{(ads)}$ on non-dissociative adsorption of imidazole were identified. The first stabilizing effect, operative for O and OH, is due to the hydrogen bond formation with the nearby adsorbed imidazole. The second stabilizing effect, relevant for O and Cl, is due to the $X_{(ads)}$ induced enhancement of the N–Cu bond between the nearby adsorbed imidazole and the surface; this effect enhances with increasing coverage of $X_{(ads)}$. The last effect is related to the $X_{(ads)}$ induced work function change and can be stabilizing (for O and Cl), negligible (for H), or destabilizing (in the case of OH) for adsorption of imidazole and explains why the impact of $X_{(ads)}$ on adsorption bonding of imidazole diminishes with the $X_{(ads)}$ coverage. Finally, if the coverage of $X_{(ads)}$ is too high, then the chemisorption of imidazole is prevented either sterically or due to the unavailability of free surface sites.

1. Introduction

Derivatives of azoles—five-membered aromatic molecules containing one nitrogen atom and at least one other heteroatom (N, O, or S)—are known for their ability to mitigate corrosion of copper and its alloys, i.e., azole compounds often act as corrosion inhibitors. It is generally accepted that a molecule must adsorb to act as an inhibitor [1]. For this reason, many computational studies, based on density-functional theory (DFT), addressed the adsorption of corrosion inhibitors on bare metal surfaces (e.g., see the recent review [2] and references therein). However, in real environments, metal surfaces are most likely never clean. Obot et al. justifiably criticized such calculations as naive because, even in the case of active dissolution, metal surfaces are likely covered with adsorbed species such as O, OH, H, and Cl [3]. To address how such species affect the adsorption of azole molecules on copper surfaces, we present herein a systematic DFT study of imidazole adsorbed on Cu(111) covered with either chemisorbed H, O, OH, or Cl. Indeed, atomistic modeling based on DFT is currently probably the best tool to investigate these kinds of issues, firstly because it is known to be able to adequately describe metal surfaces and adsorbates thereon [4], secondly because it can easily handle various hypothetical scenarios by purposely building the corresponding models "atom by atom", and thirdly because different effects can be disentangled by a proper decomposition into more basic components. This way, the effects of coverage of $X_{(ads)}$ on adsorption of imidazole and the role of the distance between imidazole and $X_{(ads)}$ can be systematically accounted for. On the contrary, the explanation of

* Corresponding author at: Department of Physical and Organic Chemistry, Jožef Stefan Institute, Jamova 39, SI-1000 Ljubljana, Slovenia.
E-mail address: tone.kokalj@ijs.si (A. Kokalj).
[1] ORCID: 0000-0002-9073-3050
[2] ORCID: 0000-0001-7237-0041

https://doi.org/10.1016/j.corsci.2022.110443
Received 5 January 2022; Received in revised form 10 June 2022; Accepted 13 June 2022
Available online 16 June 2022

such issues is more difficult by experiments due to constraints imposed by "nature", i.e., in addition to technical difficulties in maintaining atomic-level control and resolution, one is bound to adsorbate configurations that naturally form.

Although imidazole is seldom used as a corrosion inhibitor [5], it is utilized herein as an archetypal model of imidazole-based corrosion inhibitors. As for the H, O, OH, and Cl species, the first three are typically involved in cathodic corrosion reactions, whereas chloride is a well-known corrosion activator. We show herein that such species can affect the azole–surface interaction in three ways: (i) via modification of the surface work function, which in turn affects the molecule–surface bonding; this effect can either stabilize or destabilize the adsorbed molecule. (ii) Chemisorbed species, such as O and OH, can form stabilizing hydrogen bonds with adsorbed azole molecules; and (iii) chemisorbed O and Cl induce an enhancement of the N–Cu bond between the nearby adsorbed imidazole and the surface. There is at least one other effect, which is not considered herein but will be covered in the subsequent publication [6]. This effect is the aftermath of the effect (ii), i.e., once the hydrogen bond between either O or OH and nearby azole is formed, the adsorbed molecule can be further stabilized by deprotonation that involves a proton shift from the molecule to chemisorbed O or OH. This last effect is strongly supported by experimental observations showing that triazole and pyrazole deprotonate at much lower temperatures on O/Cu(100) than on bare Cu(100) [7,8].

2. Technical details

2.1. Computational method

DFT calculations were performed with the PBE+D" method that consists of the exchange-correlation functional of Perdew–Burke–Ernzerhof (PBE) [9] and a reparametrized empirical dispersion correction of Grimme, known as D2 [10]. The double prime in the PBE+D" label is used to indicate that the C_6 parameter of Cu was reparametrized from the original value of 375 Ry/Bohr^6 to the value of 140 Ry/Bohr^6 [11] to reduce the molecule–surface overbinding of the original PBE+D2 method [12–14]. Kohn–Sham orbitals were expanded in a plane-wave basis set with a kinetic energy cutoff of 30 Ry (240 Ry for the charge density). Core electrons were described with ultrasoft-pseudo potentials [15,16]. All calculations were performed with the PWscf code from the Quantum ESPRESSO distribution [17,18]. The PWTK scripting environment [19] was used to automate computational workflows.

Cu(111) was modeled by a periodic multi-slab model consisting of four (111) layers, with the bottom layer constrained to the bulk positions compatible with the calculated equilibrium bulk lattice parameter of Cu of 3.65 Å [20]. All other degrees of freedom were relaxed. Adsorbates were adsorbed on the top side of the slab. The thickness of the vacuum region—the distance from the upper Cu layer of the reference slab to the bottom layer of the slab above it—was set to about 25.5 Å, and a dipole correction of Bengtsson [21] was applied. Adsorption calculations were performed with supercells of different sizes ranging from (2 × 2) to (6 × 6). Brillouin-zone integrations were performed with the special point technique [22] using the Methfessel–Paxton smearing [23] of 0.03 Ry. Shifted $\frac{12}{n} \times \frac{12}{m} \times 1$ k-point meshes were used for the ($n \times m$) supercells, where n and m range from 2 to 6; for the (5 × 5) supercell the 3 × 3 × 1 k-point mesh was used. Spin polarization was considered for isolated atoms and radicals.

Bader charges were calculated using the `Bader` code [24,25] by generating charge densities with the projector-augmented-wave (PAW) potentials [26,27] and 1000 Ry kinetic energy cutoff for the charge density.

Molecular graphics were produced by the `xcrysden` graphical package [28]. XY plots and histograms were plotted with the `Gnuplot` program [29] and post-processing of figures was done in `Inkscape` [30].

2.2. Definitions of labels

The ImiH label is used as a shortcut for the imidazole molecule, whereas the label X is used as a generic label to designate the H, O, OH, or Cl species. The Cu(111) surface covered with a given X species is labeled as X/Cu(111), whereas imidazole adsorbed on X/Cu(111) is labeled as ImiH @ X/Cu(111).

Adsorbed X species are labeled generically as $X_{(ads)}$. To indicate to which adsorption site $X_{(ads)}$ is adsorbed, the X_{fcc}, X_{hcp}, X_{br}, and X_{top} labels are used, where the fcc and hcp subscripts stand for the face-centered-cubic and hexagonal-close-packed three-fold hollow sites, respectively, and the br and top subscripts stand for the bridge and top sites, respectively.

The surface coverage (Θ) is expressed in monolayer (ML) units, defined as the inverse of the number of surface Cu atoms per adsorbate; for example, if the ($n \times n$) supercell contains one adsorbed molecule, then the corresponding coverage of that species is $1/n^2$ ML.

2.3. Energy equations

The adsorption binding energy (E_b) was calculated as:

$$E_b = E_{A/surf} - (E_{surf} + E_A), \tag{1}$$

where A stands for the adsorbate (either ImiH, H, O, OH, or Cl) and $E_{A/surf}$ is the total energy of adsorbate/surface system, E_{surf} is the total energy of the bare slab, and E_A is the total energy of the isolated adsorbate, where H, O, OH, and Cl were treated as spin-polarized.

To address how $H_{(ads)}$, $O_{(ads)}$, $OH_{(ads)}$, or $Cl_{(ads)}$ affect the adsorption binding of imidazole, we defined ΔE_b as:

$$\Delta E_b = E'_b - E_b, \tag{2}$$

where E_b is the binding energy of imidazole on bare Cu(111), calculated with Eq. (1), whereas E'_b is the binding energy of imidazole on X/Cu (111) surface, calculated as:

$$E'_b = E_{ImiH/X/surf} - (E_{X/surf} + E_{ImiH}) \tag{3}$$

where $E_{ImiH/X/surf}$, $E_{ImiH/surf}$ and E_{ImiH} are total energies of ImiH @ X/Cu (111) coadsorption system, X/Cu(111) system, and isolated imidazole molecule, respectively.

The adsorption energies (E_{ads}) of X species were calculated with respect to isolated stable molecular species. For X = H, O, and Cl, the adsorption energies were calculated with respect to the X_2 molecule according to the reaction:

$$\mathrm{Cu(111)} + \frac{1}{2}\mathrm{X_2} \rightarrow \mathrm{X/Cu(111)}, \tag{4}$$

whereas for X = OH, the adsorption energy was calculated with respect to the water molecule according to the reaction:

$$\mathrm{Cu(111)} + \mathrm{H_2O} \rightarrow \mathrm{OH/Cu(111)} + \frac{1}{2}\mathrm{H_2}. \tag{5}$$

In contrast, for non-dissociative adsorption of imidazole, its adsorption energy is given by the binding energy E_b of Eq. (1), which corresponds to the reaction:

$$\mathrm{Cu(111)} + \mathrm{ImiH} \rightarrow \mathrm{ImiH/Cu(111)}. \tag{6}$$

Reactions (4)–(6) imply that the adsorption energies were calculated as:

$$\text{for H, O, Cl:} \quad E_{ads} = E_{X/surf} - E_{surf} - \frac{1}{2}E_{X_2}, \tag{7}$$

$$\text{for OH:} \quad E_{ads} = E_{OH/surf} + \frac{1}{2}E_{H_2} - E_{surf} - E_{H_2O}, \tag{8}$$

$$\text{for ImiH:} \quad E_{ads} = E_{ImiH/surf} - E_{surf} - E_{ImiH}. \tag{9}$$

The comparison of Eqs. (7)–(9) with Eq. (1) reveals that E_b and E_{ads} are related to each other by a constant that is specific to each adsorbate. The calculated values of these constants are:

$$\text{for H:} \quad E_{ads} = E_b + 2.25 \text{ eV}, \tag{10}$$

$$\text{for O:} \quad E_{ads} = E_b + 2.85 \text{ eV}, \tag{11}$$

$$\text{for OH:} \quad E_{ads} = E_b + 3.01 \text{ eV}, \tag{12}$$

$$\text{for Cl:} \quad E_{ads} = E_b + 1.42 \text{ eV}, \tag{13}$$

$$\text{for ImiH:} \quad E_{ads} = E_b. \tag{14}$$

2.4. Charge density, dipole moment, and work function

The electron charge density difference, $\Delta\rho(\mathbf{r})$, was used to characterize chemical bonds between the adsorbed species and the surface as well as lateral interactions between imidazole and the coadsorbed X species. Charge density difference was calculated as:

$$\Delta\rho(\mathbf{r}) = \Delta\rho_{A/surf}(\mathbf{r}) - \Delta\rho_{A}(\mathbf{r}) - \Delta\rho_{surf}(\mathbf{r}), \tag{15}$$

where the subscripts have the same meaning as defined above. Geometries of the standalone systems (A and surf) were kept consistent with that of the A/surf adsorption system. For ImiH @ X/Cu(111) coadsorption systems, electron charge densities were calculated as:

$$\Delta\rho(\mathbf{r}) = \Delta\rho_{ImiH/X/surf}(\mathbf{r}) - \Delta\rho_{ImiH}(\mathbf{r}) - \Delta\rho_{X/surf}(\mathbf{r}). \tag{16}$$

A planar integrated electron charge density difference was calculated as:

$$\Delta\rho(z) = \int_A \Delta\rho(x, y, z)\, \mathrm{d}x\, \mathrm{d}y, \tag{17}$$

where the integration runs over the area A spanned by the surface supercell, z is the surface normal direction, and $\Delta\rho(x, y, z) \equiv \Delta\rho(\mathbf{r})$. The first moment function of $\Delta\rho(z)$ was calculated as:

$$\mu(z) = \int_{-a}^{z} z' \Delta\rho(z')\, \mathrm{d}z', \tag{18}$$

where $-a$ is the z-component of the specific point in vacuum beneath the slab, such that $\Delta\rho(-a) = 0$. The first-moment function $\mu(z)$ is related to the surface normal component of the adsorption-induced dipole moment $\mu_\perp$ because for the models utilized herein—with adsorbates adsorbed only on one side of the slabs—$\mu_\perp$ can be calculated as:

$$\mu_\perp = \int_{-a}^{C-a} z\Delta\rho(z)\, \mathrm{d}z, \tag{19}$$

where C is the size of the supercell along the z-direction. Note that both $-a$ and $C - a$ are located in vacuum, such that $\Delta\rho(-a) = \Delta\rho(C - a) = 0$.

The surface normal component of the adsorption-induced dipole moment is related to the adsorption-induced work function change ($\Delta\Phi$) via the Helmholtz relation (in atomic Hartree units):

$$\Delta\Phi = 4\pi\theta e\mu_\perp, \tag{20}$$

where $\mu_\perp$ is expressed in e Bohr unit, θ is the adsorbate coverage (in Bohr^{-2}), and e stands for the elementary charge ($e = 1$ e). Note that among currently considered $X_{(ads)}$ only OH possesses a permanent molecular dipole and to capture it by $\mu_\perp$, the respective $\Delta\rho(z)$ was calculated as:

$$\Delta\rho(z) = \rho_{OH/surf}(z) - \rho_{O}(z) - \rho_{H}(z) - \rho_{surf}(z). \tag{21}$$

The adsorption induced work function change can be obtained from Eq. (20) that in turn utilizes Eqs. (16)–(19). While these equations are very useful for a detailed analysis, they are cumbersome for routine calculation of $\Delta\Phi$ because they require additional post-processing calculations. For the models utilized herein, with adsorbates adsorbed only on one side of the slabs, $\Delta\Phi$ can be straightforwardly obtained from the PWscf output provided that the dipole correction was used. In this case, $\mu_\perp$ of Eq. (20) is opposite to the self-consistently determined dipole of the counteracting dipole layer utilized in the dipole correction.

3. Results and discussion

3.1. Adsorption on bare Cu(111)

Imidazole prefers to adsorb on a top site of Cu(111) by forming the N–Cu bond with its N3 atom [31–33] (Fig. 1). Among the possible orientations of imidazole around the N–Cu bond (i.e., the "helicopter" orientation), the staggered orientation is predicted to be marginally more stable than the eclipsed one (by 0.01 eV, Fig. 1). In the smallest considered (2 × 2) supercell, only the staggered orientation is viable because molecules better avoid each other in this orientation.

H, O, OH, and Cl species prefer to adsorb onto three-fold hollow sites (Table 1). Among the two hollow sites, the fcc hollow site is marginally preferred over the hcp site, except for O where the difference is somewhat more significant (about 0.1 eV).

The dependence of adsorption energy on the coverage of H, O, OH, and Cl species as well as of an imidazole molecule on bare Cu(111) is shown in Fig. 2, where supercells from (2 × 2) to (6 × 6) are considered, corresponding to coverage ranging from 1/4 to 1/36 ML, respectively. Only the most stable sites (top site for imidazole and fcc site for the X species) are considered, except for OH where the less stable bridge site is also considered because we observed that in some cases OH_{fcc} shifts to OH_{br} upon adsorption of imidazole. While the adsorption energy of imidazole displays a strong dependence on the coverage (the binding energy enhances by about 0.3 eV as passing from 1/4 to 1/36 ML coverage), the adsorption energies of X species are rather insensitive to the coverage; the only exception is OH_{fcc} at 1/4 ML that displays by about 0.1 eV more endothermic E_{ads} compared to lower coverages.

The reason the adsorption energy of imidazole and, to a smaller extent, of OH_{fcc} depends on the coverage can be attributed to lateral dipole–dipole interactions. Indeed, it is known that imidazole displays long-range lateral dipolar interactions due to its large permanent dipole moment [31].[3] A similar argument can also explain slightly weaker adsorption of OH_{fcc} at the high coverage of 1/4 ML, i.e., among the adsorbed X species, OH_{fcc} displays the largest adsorption-induced change of the work function (Fig. 3) and, consequently, the largest surface normal component of the dipole (cf. Eq. (20)). It also protrudes

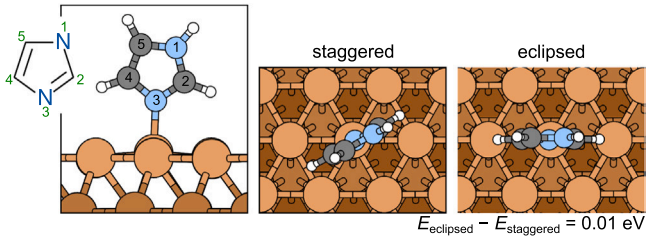

Fig. 1. Top and side view snapshots of imidazole adsorbed on Cu(111); skeletal structure of imidazole and its atom numbering are also shown. Staggered and eclipsed "helicopter" orientations of imidazole are considered. In the eclipsed orientation, the molecular plane is aligned such that the C2–H and C4–H bonds point to the neighboring Cu atoms, whereas in the staggered orientation, the C2–H and C4–H bonds point to the bridge sites in between the neighboring Cu atoms. Among the two orientations, the staggered one is marginally more stable, by 0.01 eV.

[3] The DFT calculated value of dipole moment of imidazole is 3.8 D [31,34].

Table 1
Adsorption binding energies (E_b) and adsorbate heights (h) for H, O, OH, and Cl at high-symmetry adsorption sites on (2 × 2)–Cu(111). The reported h values correspond to the z-coordinate difference between the adsorbate and the average height of the Cu atoms to which the adsorbate binds; for diatomic OH, the z-coordinate of the O atom is taken. Note that some high-symmetry adsorption sites are not local minima and for some of them the values were obtained with constrained relaxation.

	E_b (eV)				h (Å)			
	fcc	hcp	bridge	top	fcc	hcp	bridge	top
H	−2.50	−2.49	−2.35	−1.87	0.91	0.93	1.06	1.53
O	−4.50	−4.39	−4.00[a]	−2.71	1.12	1.13	1.22[a]	1.76
OH	−2.98	−2.95	−2.87	−2.41	1.38	1.40	1.51	1.88
Cl	−3.39	−3.38	−3.30	−3.00	1.87	1.88	1.93	2.19

[a]Calculated with the constrained relaxation.

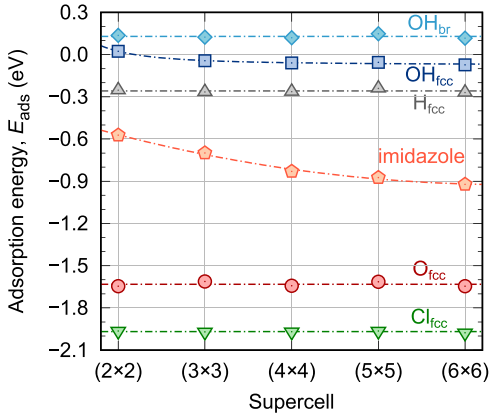

Fig. 2. Adsorption energies (E_{ads}) for considered species on Cu(111) as a function of the ($n \times n$) supercell size, corresponding to the adsorbate coverage of $1/n^2$ ML.

out of the surface more than the other X species, hence its dipolar interactions are less screened by the metal than those of the other adsorbates, which are located closer to the surface.

Fig. 3 reveals that $O_{(ads)}$ and $Cl_{(ads)}$ increase the work function, $H_{(ads)}$ has almost no effect on it, whereas $OH_{(ads)}$ decreases the work function. The figure reveals that the adsorption-induced change of the work function depends linearly on the adsorbate coverage, a trend expected from the Helmholtz Eq. (20). The adsorption-induced increase of the work function is usually associated with a negative charge of adsorbates located above the surface. The plots of electron charge density difference of the X/Cu(111) systems (Fig. 4) reveal that all X adsorbates are

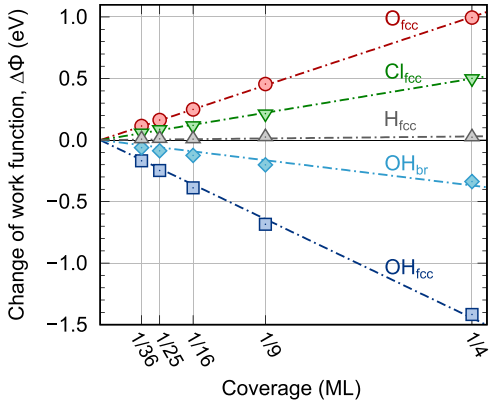

Fig. 3. Adsorption induced work function change (ΔΦ) of chemisorbed H_{fcc}, O_{fcc}, OH_{fcc}, OH_{br}, and Cl_{fcc} on Cu(111) as a function of the adsorbate coverage.

negatively charged, and this qualitative observation is confirmed by the calculated Bader charges (also reported in Fig. 4). It is worth noting that $H_{(ads)}$ is negatively charged, which is in stark contrast with cases where H adsorbs to an O atom at oxide surfaces (thus forming an OH group) and is proton-like. The reason that $H_{(ads)}$ has a negligible effect on the work function of Cu(111), despite its negative charge, can be attributed to a slight depletion of electron charge, seen in Fig. 4 as a very faint bluish region located above the pronounced red charge accumulation region. This electron charge depletion is much more visible in the planar integrated charge density difference $\Delta\rho(z)$, shown in Fig. 5a. Without this depletion, the negatively charged $H_{(ads)}$ atom would increase the work function as shown by the corresponding analysis of $\Delta\rho(z)$ and its first-moment function $\mu(z)$ in Fig. 5a. For $O_{(ads)}$, this charge depletion is largely missing (Fig. 5b) and, correspondingly, $O_{(ads)}$ increases the work function. Similarly, the decrease of the work function induced by $OH_{(ads)}$ can be attributed to its outward-pointing H atom that is positively charged (Fig. 5c). OH_{fcc} has a higher effect on the work function than OH_{br} because its polar O–H bond points normal to the surface, whereas for OH_{br}, the O–H bond is tilted (cf. Fig. 4).

3.2. Adsorption of imidazole on X/Cu(111)

In this section, we characterize the effect of the pre-adsorbed X species on the adsorption of imidazole. As shown above, imidazole prefers to adsorb on a top site, and the X species prefer to adsorb onto fcc sites (Table 1), hence we considered the adsorption of imidazole on a top site with one X species pre-adsorbed onto an fcc hollow site per ($n \times n$) supercell, with n ranging from 2 to 6. While on bare Cu(111), all top adsorption sites are equivalent, for X_{fcc}/Cu(111), the number of symmetry inequivalent top sites increases with the supercell size. To make the symmetry of the ($n \times n$)–X_{fcc}/Cu(111) systems more apparent, Fig. 6 plots them in the form of colored hexagons, where the symmetry inequivalent top sites are color-coded. For such systems, we realized that the number of symmetry inequivalent top sites (N_{ineq}) is given by the expression:

$$N_{ineq} = n + \sum_{i=1}^{n} \mathrm{int}\left(\frac{i-1}{3}\right), \tag{22}$$

where n corresponds to the ($n \times n$) supercell and int(j/k) stands for the integer division of j by k. The validity of this equation was verified numerically up to the (1000 × 1000) supercell, which is more than enough for all practical purposes. The dependence of the number of symmetry inequivalent top sites on the supercell size is shown graphically in Fig. 7, whereas Fig. 8 schematically plots the lateral distance from the position of the central fcc site to a given top site for all the inequivalent sites up to the largest considered (6 × 6) supercell.

To scrutinize the effect of the adsorbed X species (X = H, O, OH, or Cl) on the adsorption of imidazole on Cu(111), a large number of different adsorption geometries were considered at each supercell dimension. The configurational search involved all inequivalent top adsorption sites for each considered supercell. At each site, different orientations of imidazole were probed (note from Fig. 1 that the difference between staggered and eclipsed "helicopter" orientation of imidazole is only 0.01 eV, which implies that the presence of $X_{(ads)}$ can easily alter the orientation). In total, about 400 different adsorption configurations were considered. The corresponding results are presented in Fig. 9, where the effect of pre-adsorbed X species on the adsorption of imidazole is evaluated using ΔE_b of Eq. (2). For ease of discussion, this effect is referred to as the X coadsorption effect, and the top adsorption sites are referred to by the colors defined in Fig. 6. In Fig. 9 only the systems consisting of one adsorbed imidazole molecule and one adsorbed X species per ($n \times n$)–Cu(111) supercell are considered. The most stable orientations of imidazole at different top sites of X/Cu(111) up to the green site are shown in Fig. 10. For sites beyond the green sites, different helicopter orientations of imidazole display similar stability

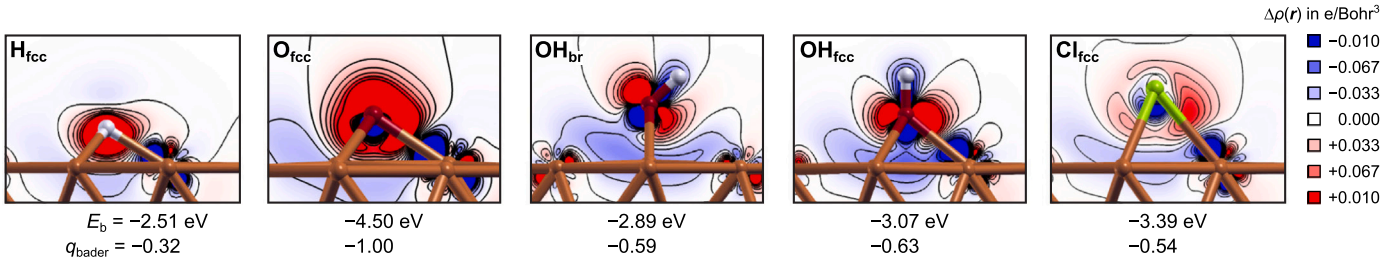

Fig. 4. Electron charge density difference, $\Delta\rho(\mathbf{r})$ of Eq. (15), for H_{fcc}, O_{fcc}, OH_{br}, OH_{fcc}, and Cl_{fcc} on (4 × 4)–Cu(111). Eleven contours are drawn in a linear scale from −0.01 to +0.01 e/Bohr^3 with the increment of 0.002 e/Bohr^3. Electron excess regions are colored red and electron deficit regions are blue (i.e., electrons flow from blue to red regions). The corresponding binding energies and adsorbate Bader charges are also stated (negative values correspond to negatively charged adsorbates).

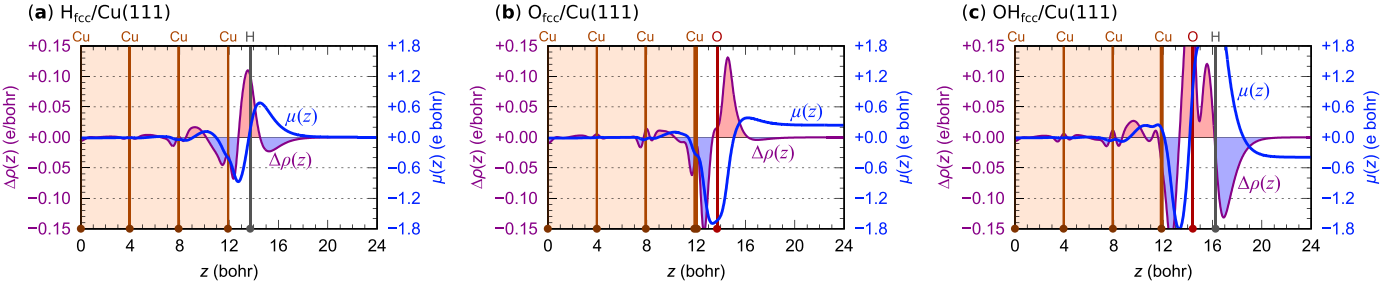

Fig. 5. Planar integrated electron charge density difference $\Delta\rho(z)$ (purple curve), defined by Eq. (17), and the first moment function $\mu(z)$ (blue curve), defined by Eq. (18), for H_{fcc}, O_{fcc}, and OH_{fcc} on (4 × 4)–Cu(111). Note that $\Delta\rho(z)$ of OH_{fcc} was calculated as $\Delta\rho(z) = \rho_{OH/surf}(z) - [\rho_O(z) + \rho_H(z) + \rho_{surf}(z)]$; the reason that $\rho_O(z) + \rho_H(z)$ was used instead of $\rho_{OH}(z)$ is to capture also the permanent dipole of OH. The z positions of the Cu layers and adsorbate atoms are indicated by vertical lines. The surface normal component of the adsorbate dipole moment $\mu_\perp$ (i.e., adsorption-induced for H_{fcc} and O_{fcc} and permanent + adsorption-induced for OH_{fcc}) equals the value of $\mu(z)$ on the right side of the plot.

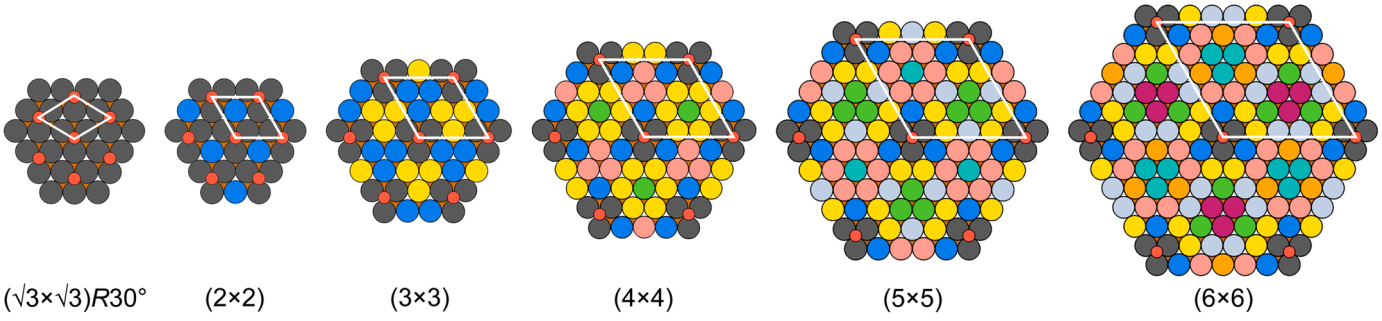

Fig. 6. Schematic presentation of inequivalent top adsorption sites for the $(\sqrt{3} \times \sqrt{3})R30^\circ$ and $(n \times n)$–X_{fcc}/Cu(111) systems, with n ranging from 2 to 6. Reference supercells are indicated by white parallelograms. The coverage of $X_{(ads)}$ is 1/3 ML for $(\sqrt{3} \times \sqrt{3})R30^\circ$ and $1/n^2$ ML for $(n \times n)$ supercells. Small reddish balls represent the X_{fcc} adsorbates, whereas larger balls are the Cu atoms. Cu atoms (i.e., top adsorption sites) that are related by symmetry are colored with the same color.

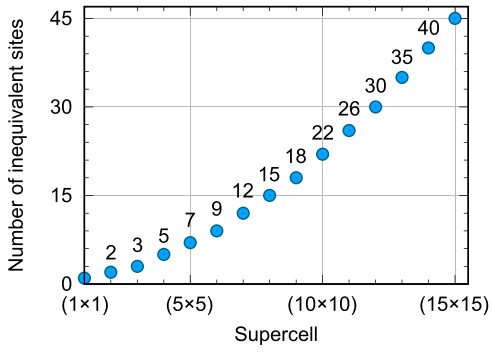

Fig. 7. Number of symmetry inequivalent top sites for the $(n \times n)$–X_{fcc}/Cu(111) systems as a function of the supercell size (cf. Eq. (22)).

due to the long distance between $X_{(ads)}$ and imidazole. The results in Fig. 9 reveal that the X coadsorption effect depends on the type and the coverage of the X species as well as the distance between the adsorbed imidazole and $X_{(ads)}$. On the nearest gray adsorption sites, $H_{(ads)}$ destabilizes imidazole adsorption by 0.14 eV (not shown in Fig. 9), whereas the other considered $X_{(ads)}$ species prevent the adsorption of imidazole thereon, which is not surprising because these sites are too close to the adsorbed X species, i.e., they are laterally only 1.5 Å away from the fcc site to which the X species is adsorbed. Even for $H_{(ads)}$, there is a pronounced tendency to avoid imidazole adsorption at the gray site by displacing either imidazole or $H_{(ads)}$ to a neighboring site to increase the distance between the two coadsorbates. Gray sites are therefore not considered in Fig. 9 (note that the smallest $(\sqrt{3} \times \sqrt{3})R30^\circ$ supercell shown in Fig. 6 consists of only gray sites, hence it is not considered in Fig. 9).

A simple analysis in terms of the sizes of the X species and the imidazole molecule reveals that, with respect to the lateral intersite

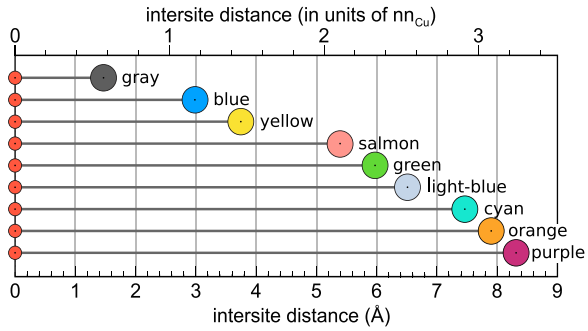

Fig. 8. Schematic presentation of the lateral intersite distance between the position of the central fcc site (small reddish balls) and a given top site (larger balls, colored according to Fig. 6) for all the inequivalent top sites up the largest considered (6 × 6) supercell. The top abscissa axis represents the intersite distance in units of the Cu–Cu nearest neighbor distance (nn_{Cu}). The names of the color sites are also explicitly stated.

distance, the surface sites can be classified into three regions: (i) Pauli repulsion region, consisting of the nearest neighbor gray sites, where imidazole cannot adsorb for X = O, OH, and Cl;[4] (ii) local region, consisting of blue and yellow sites, where H-bonds between the X species and imidazole are possible; and (iii) distant region consisting of remaining sites. These sites are too far for the formation of X···imidazole H-bonds (they are more than 5.3 Å away from the central fcc site, Fig. 8).

The ΔE_b results of Fig. 9 reveal that among the considered X species, $O_{(ads)}$ displays the largest effect on the adsorption of imidazole, i.e., it enhances the adsorption binding of imidazole ($\Delta E_b < 0$). $Cl_{(ads)}$ also enhances the adsorption of imidazole (except at high coverage of 1/4 ML corresponding to (2 × 2)–Cl_{fcc} overlayer) but to a lesser extent than $O_{(ads)}$. $H_{(ads)}$ affects the adsorption of imidazole insignificantly, whereas $OH_{(ads)}$ usually diminishes the adsorption binding of imidazole.

At low $X_{(ads)}$ coverage, imidazole prefers to adsorb near $X_{(ads)}$ to either blue or yellow sites irrespective of whether $X_{(ads)}$ enhances or diminishes the adsorption binding of imidazole, except in the case of $H_{(ads)}$, where imidazole binds very similarly to all non-gray sites because $H_{(ads)}$ has almost no effect on the adsorption of imidazole. In general, the coadsorption effect of $X_{(ads)}$ diminishes with the coverage, irrespective of the adsorption site. The only exceptions are the (2 × 2)–OH and (3 × 3)–OH overlayers that affect the adsorption binding energy of imidazole to a lesser extent than the lower coverage OH configurations.

Below, the coadsorption effects of $O_{(ads)}$, $Cl_{(ads)}$, and $OH_{(ads)}$ are described in more detail, whereas $H_{(ads)}$ is excluded from a more detailed description because it affects the adsorption of imidazole insignificantly.

3.2.1. *Coadsorption effect of $O_{(ads)}$*

Among the considered X species, $O_{(ads)}$ displays the strongest and the most stabilizing effect on the adsorption of imidazole. The stabilizing effect is particularly strong for the nearby yellow and blue sites due to the formation of an H-bond between imidazole and $O_{(ads)}$ (vide infra). Among the cases considered in Fig. 9, the stabilizing effect is the largest at the high coverage of 1/4 ML, corresponding to the (2 × 2) supercell, where the binding of imidazole is enhanced by about 0.5 eV, whereas at low $O_{(ads)}$ coverages the stabilization drops to about 0.25 eV.

That $O_{(ads)}$ can stabilize adsorption of azoles was also proven by experiments. In particular, Cho et al. [35] demonstrated with STM that on Cu(110) with co-existing phases of clean Cu(110) and

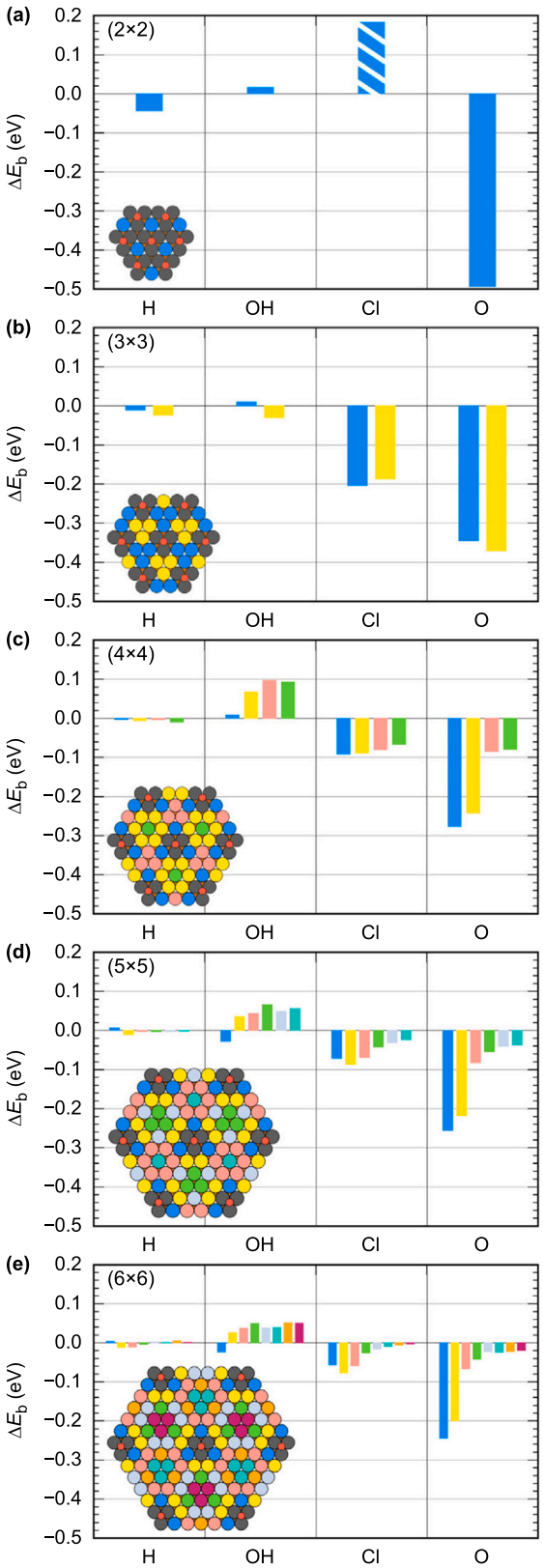

Fig. 9. The effect of adsorbed H, OH, Cl, or O species on the adsorption of imidazole on Cu(111) as measured by ΔE_b of Eq. (2). Histograms represent the ΔE_b values of the most stable identified systems for each considered case. Bars are colored according to the top site color coding of Fig. 6. The blue bar corresponding to (2 × 2)–Cl/Cu(111) is stripped because in this case imidazole does not adsorb via N–Cu bonding (see Fig. 11).

[4] At the $X_{(ads)}$ coverage of at least 1/3 ML—as exemplified by the $(\sqrt{3} \times \sqrt{3})R30^{\circ}$ structure—only gray sites exist (Fig. 6). This implies that at so high $X_{(ads)}$ coverage, imidazole cannot adsorb for X = O, OH, and Cl. It will be shown later that imidazole can adsorb on Cu(111) covered with 1/3 ML or even 1/2 ML of $O_{(ads)}$ if some O adatoms displace from fcc to hcp sites and thus make some top sites non-gray.

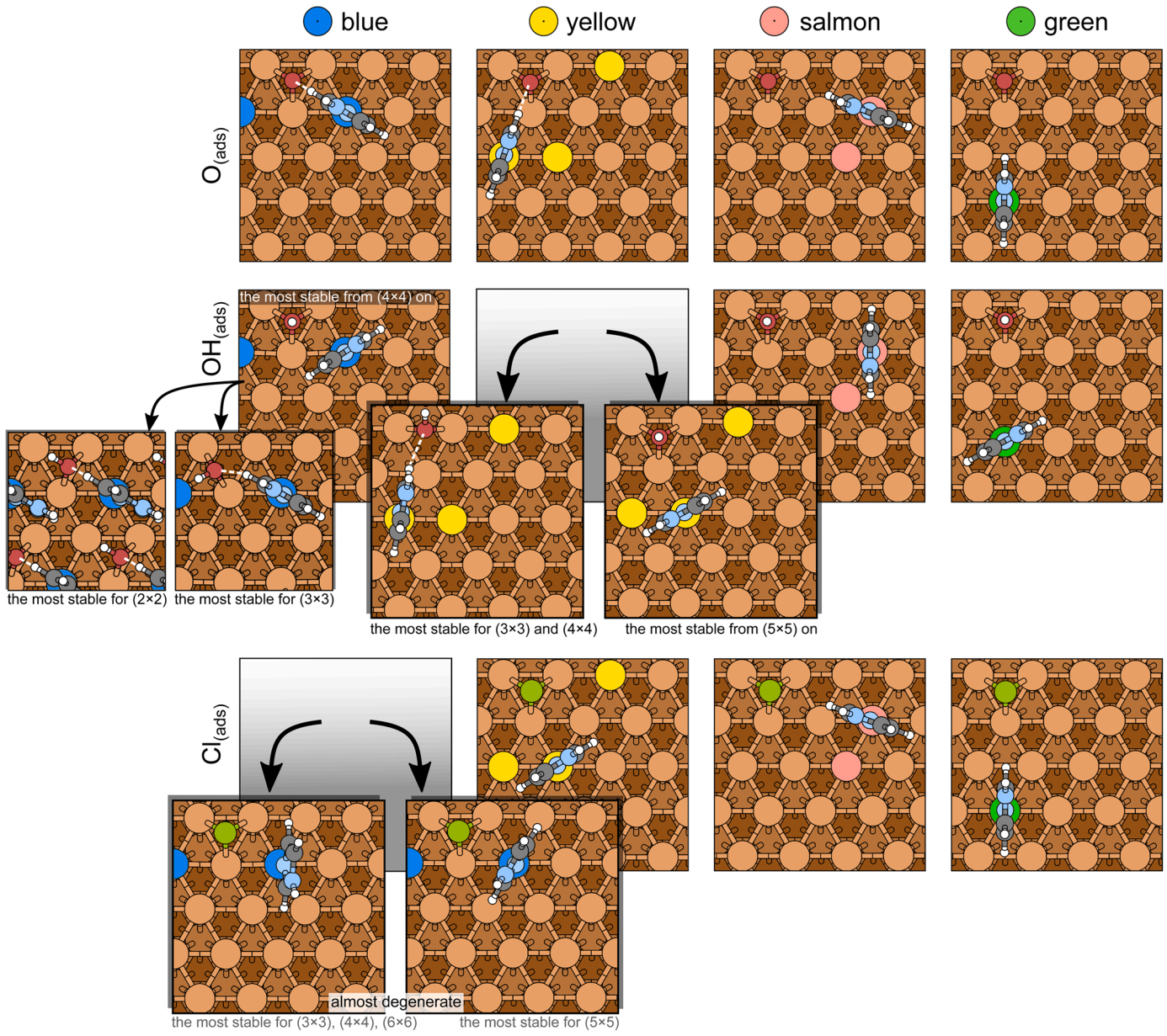

Fig. 10. Top-view snapshots of the most stable identified structures of imidazole adsorbed (from left to right) on blue, yellow, salmon, and green top sites (from top to bottom) on O/Cu(111), OH/Cu(111), and Cl/Cu(111). At each column, all the equivalent top sites of the specific color are so colored. For some cases, the stablest structure depends on the supercell size, and for those cases all such structures are shown.

oxygen-reconstructed Cu(110)–(2 × 1), benzotriazole preferentially adsorbs on the oxygen-reconstructed phase.

3.2.2. *Coadsorption effect of $Cl_{(ads)}$*

The (2 × 2)–$Cl_{(ads)}$ overlayer, corresponding to the coverage of 1/4 ML, significantly destabilizes the adsorption of imidazole, whereas at lower considered coverages, the effect changes, and $Cl_{(ads)}$ stabilizes imidazole adsorption, but to a lesser extent than $O_{(ads)}$. The reason (2 × 2)–$Cl_{(ads)}$ overlayer destabilizes adsorption of imidazole is that $Cl_{(ads)}$ is too bulky[5] to allow imidazole to come close to the copper surface (see the top-view snapshot of Fig. 11a) and, consequently, imidazole is located over 3 Å above the surface Cu-layer (the corresponding N–Cu distance is about 3.9 Å). The side-view snapshot of this structure (Fig. 11a) reveals that imidazole adsorbs considerably different than in other lower coverage cases (Fig. 11b), where it forms a direct N–Cu bond, about 2.1 Å long.

As for the lower Cl coverages, where the adsorption of imidazole is stabilized, the nearby sites are only marginally preferred over the distant sites because, in contrast to $O_{(ads)}$, H-bonds between imidazole and $Cl_{(ads)}$ do not form. At the nearby yellow and blue sites, imidazole orients with its H atoms away from $Cl_{(ads)}$ (see the corresponding snapshots in Fig. 10). The salmon site is the first site where imidazole orients with its C–H bond toward $Cl_{(ads)}$, and the resulting electrostatic interaction is likely the reason that the salmon site is of very similar stability as the blue and yellow sites.

At first glance, the finding that $Cl_{(ads)}$ stabilizes the adsorption of azoles seems to contradict experimental observations that chloride ions displace adsorbed benzotriazole from a copper surface [37]. Using a series of experiments, Yang et al. [37] estimated Gibbs adsorption energies as a function of electrode potential and found that at negative

[5] $Cl_{(ads)}$ is the bulkiest among the considered $X_{(ads)}$ species; the ionic radius of Cl^- is 1.81 Å, whereas the ionic radius of O^{2-} ranges from 1.21 to 1.42 Å [36].

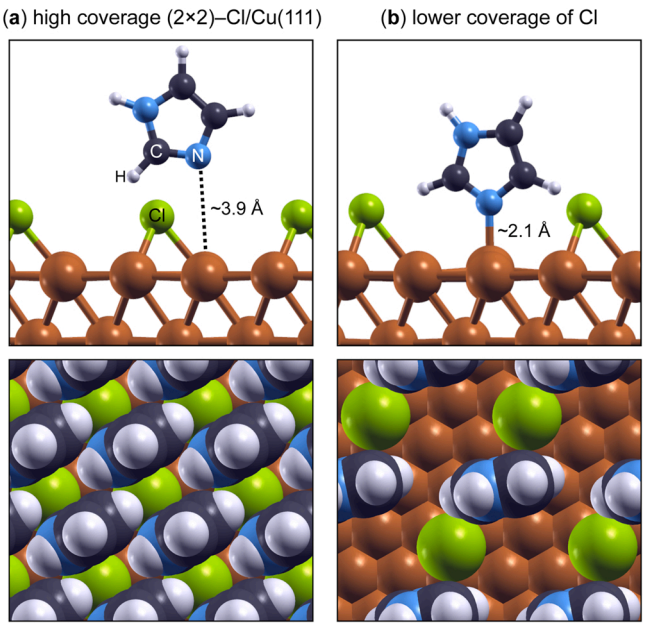

Fig. 11. Side-view and top-view snapshots of imidazole structures at (a) high-coverage (2 × 2)–Cl/Cu(111) and (b) lower 1/9 ML $Cl_{(ads)}$ coverage. In the top-view snapshots, atoms are drawn with the van der Waals radii. The top-view snapshot in (a) reveals that $Cl_{(ads)}$ is too bulky to allow imidazole to come close to the copper surface in the case of (2 × 2)–$Cl_{(ads)}$ overlayer and, consequently, the N–Cu distance is about 3.9 Å long, whereas at a lower Cl coverage imidazole forms about 2.1 Å long N–Cu bond with the surface.

potentials vs. Ag/AgCl the adsorption of benzotriazole is more exergonic than that of Cl^-, whereas at positive potentials the two energies become similar; only at potentials around 0 V vs. Ag/AgCl the adsorption of Cl^- is slightly more exergonic than that of benzotriazole. The reason for Cl^- displacing benzotriazole from the surface can thus be attributed to the concentration of the two species in solution, which is typically higher for chlorides. At a high chloride concentration (0.5 M in Ref. [37]), the tendency for Cl^- adsorption is very strong, hence an optimal saturation structure on Cu(111) is most likely formed, which is the high coverage 1/3 ML $(\sqrt{3}\times\sqrt{3})R30^\circ$–Cl/Cu(111) phase [38,39] (see Fig. S1b in the Supplementary material). According to our results, azoles cannot adsorb at such a high Cl coverage, thus corroborating experimental observations [37]; note that already the 1/4 ML (2 × 2)–Cl/Cu(111) structure sterically prevents the adsorption of imidazole (cf. Fig. 11a).

A beneficial effect of chlorides on the formation of organic film on a copper surface was reported by Kozlica et al. [40] who showed that Cl^- ions act both as a promoter and a reactant for the formation of a polymerized Cu–Cl–mercaptobenzimidazole film[6] that remarkably protects the copper from corrosion, whereas in the absence of chloride ions, the formed polymerized Cu–mercaptobenzimidazole film shows considerably inferior corrosion protection. While this example is far from the current case of coadsorbed $Cl_{(ads)}$ and imidazole on Cu(111), it shows that chloride ions can act beneficially in specific cases.

3.2.3. Coadsorption effect of $OH_{(ads)}$

$OH_{(ads)}$ usually diminishes the adsorption binding of imidazole, particularly for distant sites. Only in three cases involving the nearby sites, $OH_{(ads)}$ slightly enhances the adsorption binding of imidazole, i.e., at the yellow site of (3 × 3)–OH as well as at the blue sites of (5 × 5)–OH and (6 × 6)–OH. When imidazole adsorbs on the blue sites of (2 × 2)–OH and (3 × 3)–OH as well as on yellow sites of (3 × 3)–OH and (4 × 4)–OH, the OH groups displace from the preferred fcc sites to the inferior bridge sites as to form CH···OH hydrogen bonds with imidazole molecules. Note that the H atom of OH must point away from imidazole for the CH···OH hydrogen bond to develop, and this is possible only for tilted OH_{br} and not for perpendicular OH_{fcc}.

An interesting observation about the coadsorption effect of $OH_{(ads)}$ is that when the most stable imidazole adsorption site at a given $OH_{(ads)}$ coverage is considered, $OH_{(ads)}$ has a negligible effect on the adsorption binding energy of imidazole as it affects it to within ±0.03 eV.

3.3. Electron charge density difference of ImiH @ X/Cu(111)

As tentatively explained above, one reason that $O_{(ads)}$ considerably enhances the adsorption bonding of imidazole on Cu(111) is the formation of a hydrogen bond between $O_{(ads)}$ and imidazole. Therefore, the binding enhancement induced by $Cl_{(ads)}$ is smaller than that of $O_{(ads)}$ because $Cl_{(ads)}$ does not form such hydrogen bonds. This reasoning is supported by the plots of the electron charge density difference of imidazole on bare and X-covered Cu(111) shown in Fig. 12. In all cases, the formation of a direct N–Cu chemical bond is evident by the red electron accumulation lobe in the middle of the N–Cu bond. This is a clear sign of chemisorption [41]. The figure further reveals that a CH···O hydrogen bond forms between imidazole and $O_{(ads)}$. In contrast, such a hydrogen bond is missing in the case of $Cl_{(ads)}$ because at the nearby blue and yellow sites, imidazole orients with its H atoms away from $Cl_{(ads)}$ (see Fig. 10); the salmon site is the first one where imidazole orients with its C–H bond toward $Cl_{(ads)}$, but the corresponding H···Cl distance of 3.6 Å is too long for hydrogen bonding (the lack of hydrogen bonding, in this case, is evident from the $\Delta\rho(\mathbf{r})$ plot shown in Fig. S2 in the Supplementary material). Fig. 12 further reveals that a weak CH···O hydrogen bond also forms between imidazole and OH_{br}, whereas in the case of OH_{fcc} such a hydrogen bond is missing and imidazole orients with its H atoms away from OH_{fcc}. The formation of such a hydrogen bond is the reason that, in some cases, OH shifts from the fcc to the bridge site, which implies that the cost of displacing OH from the stablest fcc to the inferior bridge site (cf. Table 1) is compensated by the formation of the hydrogen bond.

In addition to the hydrogen bond between $O_{(ads)}$ and imidazole, Fig. 12 shows that the presence of $O_{(ads)}$ and $Cl_{(ads)}$ also strengthens the N–Cu bond as evidenced by the enhanced red electron accumulation lobe in the middle of the N–Cu bond and by the shortened N–Cu bond (e.g., compare Fig. 12a with Figs. 12c and 12f). In contrast, no such enhancement of the charge accumulation is evident in the case of $H_{(ads)}$ and $OH_{(ads)}$. This charge accumulation enhances as the coverage of $O_{(ads)}$ increases and the N–Cu bond concomitantly shortens, as evident from the top row plots of Fig. 13, where the $O_{(ads)}$ coverages of 0, 1/16, and 1/4 ML are considered, while the coverage of imidazole is held constant at 1/16 ML. Note that this enhancement of charge accumulation is present only at nearby sites but not at the distant green site (see the bottom row plot in Fig. 13). Hence, not only the coverage but also the distance from $O_{(ads)}$ matters.

3.4. Coadsorption effect: Equivalent coverage of imidazole and $X_{(ads)}$

To summarize the contribution of the pre-adsorbed $X_{(ads)}$ species on the adsorption binding energy of imidazole and the dependence of E_b on the coverage, Fig. 14 compares the imidazole E_b values of the most stable identified ImiH @ X/Cu(111) structures to those obtained on bare Cu (111) for each considered coverage. Here the data associated with Fig. 9 are utilized, hence only ImiH @ X/Cu(111) systems that contain one adsorbed imidazole molecule and one adsorbed X species per ($n \times n$)–Cu (111) supercell are considered, i.e., the coverage of imidazole and $X_{(ads)}$ is the same. This figure clearly shows that $O_{(ads)}$ (red curve) considerably enhances the adsorption bonding of imidazole, and so does $Cl_{(ads)}$ (green curve), although to a lesser extent and only to the point where there is

[6] Such a polymerized film formed on copper immersed into 3 wt% NaCl solution containing 1 mM mixture of mercaptobenzimidazole and octylphosphonic acid in the molar ratio of 9:1.

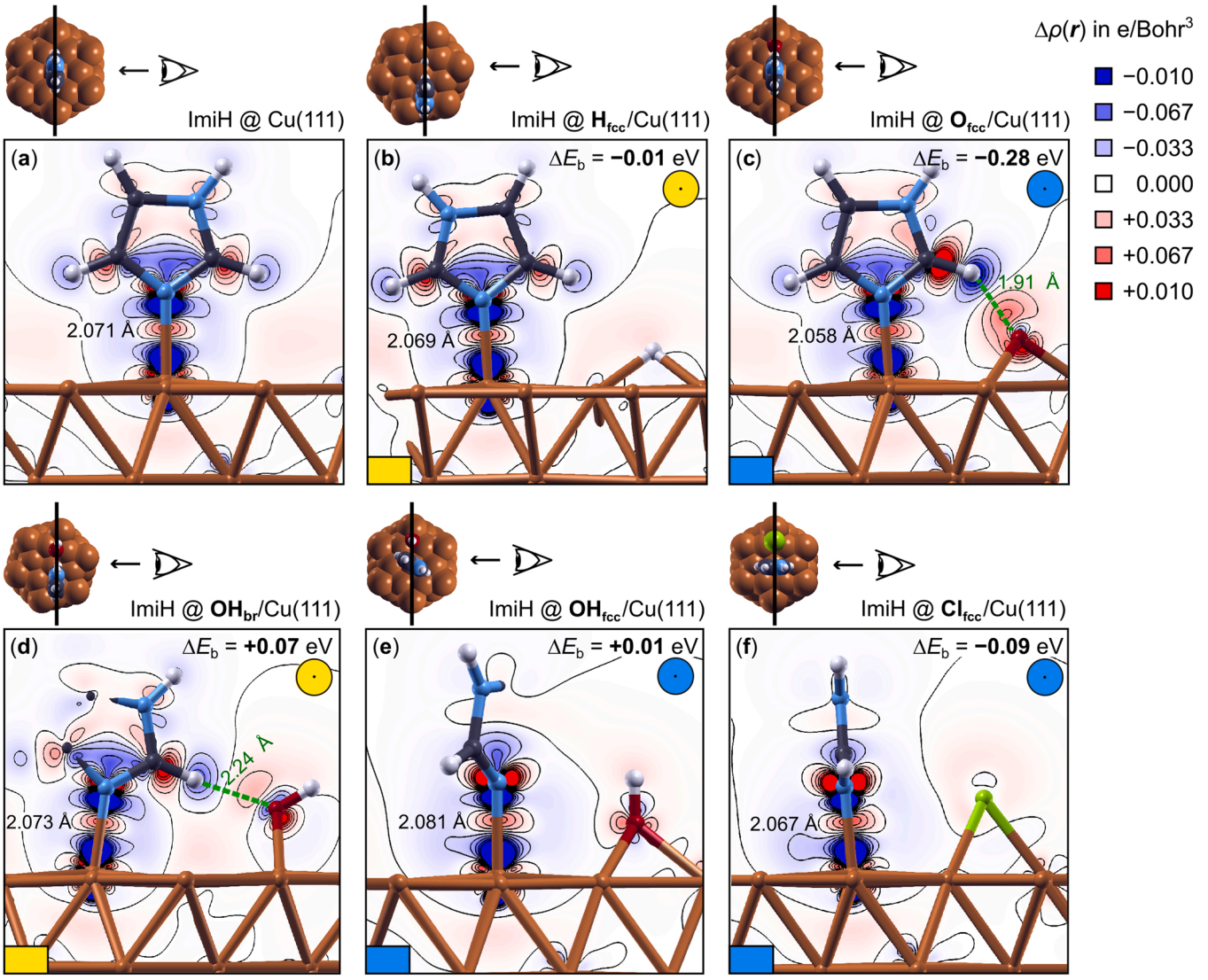

Fig. 12. Electron charge density difference, $\Delta\rho(\mathbf{r})$ of Eq. (16), for imidazole adsorbed either at blue or yellow sites on (4 × 4)–X/Cu(111), X = H, O, OH, and Cl. The $\Delta\rho(\mathbf{r})$ of imidazole on bare (4 × 4)–Cu(111) is also shown for comparison. Eleven contours are drawn in a linear scale from −0.01 to +0.01 e/Bohr^3 with the increment of 0.002 e/Bohr^3. Electron excess regions are colored red, and electron deficit regions are blue (i.e., electrons flow from blue to red regions). The corresponding ΔE_b values and characteristic bond lengths are also stated. The small hexagonal snapshots above the $\Delta\rho(\mathbf{r})$ plots indicate the positions of the contour planes, whereas the small colored circles at the top-right (also colored rectangles at the bottom-left) of the $\Delta\rho(\mathbf{r})$ plots indicate the type of adsorption site of imidazole.

enough space in between Cl adatoms for imidazole to adsorb unhindered. In contrast, $H_{(ads)}$ and $OH_{(ads)}$ affect the adsorption of imidazole negligibly, which is why the respective E_b values fall within the thick brownish curve (Fig. 14) that represents the values obtained on bare Cu (111) as well as on H/Cu(111) and OH/Cu(111).

3.5. Non-equivalent coverage of imidazole and $X_{(ads)}$

Up to this point, the same coverage of $X_{(ads)}$ and imidazole was considered, i.e., one $X_{(ads)}$ species and one imidazole molecule per ($n \times n$)–Cu(111) supercell (the only exception is the rightmost $\Delta\rho(\mathbf{r})$ plot in Fig. 13) and the results revealed that the magnitude of the coadsorption effect depends on the coverage (for example, the effect of $O_{(ads)}$ is the largest at the highest considered coverage and diminishes as the coverage of $O_{(ads)}$ decreases). However, such a setup does not provide an answer to the question of whether the effect of $X_{(ads)}$ on ΔE_b depends on the coverage of both $X_{(ads)}$ and imidazole or only on the coverage of $X_{(ads)}$. To answer this question, we performed a series of calculations, where the coverage of $O_{(ads)}$ was held constant at 1/4 ML, and the coverage of imidazole was varied from 1/4 ML to 1/36 ML. A similar strategy was also utilized for $Cl_{(ads)}$. The corresponding results, presented in Fig. 15, reveal that the effect of $X_{(ads)}$ on ΔE_b is largely invariant to the coverage of imidazole—irrespective of the coverage of imidazole, the corresponding values of ΔE_b are -0.50 ± 0.01 eV for (2 × 2)–O/Cu(111), -0.34 ± 0.02 eV for (2 × 3)–Cl/Cu(111), and -0.19 ± 0.01 eV for (3 ×3)–Cl/Cu(111)—although, due to long-range dipolar interactions, the E_b values of imidazole become more exothermic as the coverage of imidazole reduces, e.g., for (2 × 2)–O/Cu (111) the binding of imidazole strengthens from −1.06 eV at 1/4 ML to −1.43 eV at 1/36 ML of imidazole.

Having established that ΔE_b of imidazole is largely invariant to the coverage of imidazole, we now examine how ΔE_b depends on the coverage of $X_{(ads)}$. To this end, Fig. 16 plots the dependence of ΔE_b of imidazole on the coverage of $O_{(ads)}$ and $Cl_{(ads)}$; here, only the most stable adsorption structures of imidazole are considered, which involve either blue or yellow sites for O/Cu(111) and Cl/Cu(111) (cf. Fig. 9). In addition to the data from Fig. 9, several other structures are also considered in Fig. 16, where the coverage of imidazole is lower than the

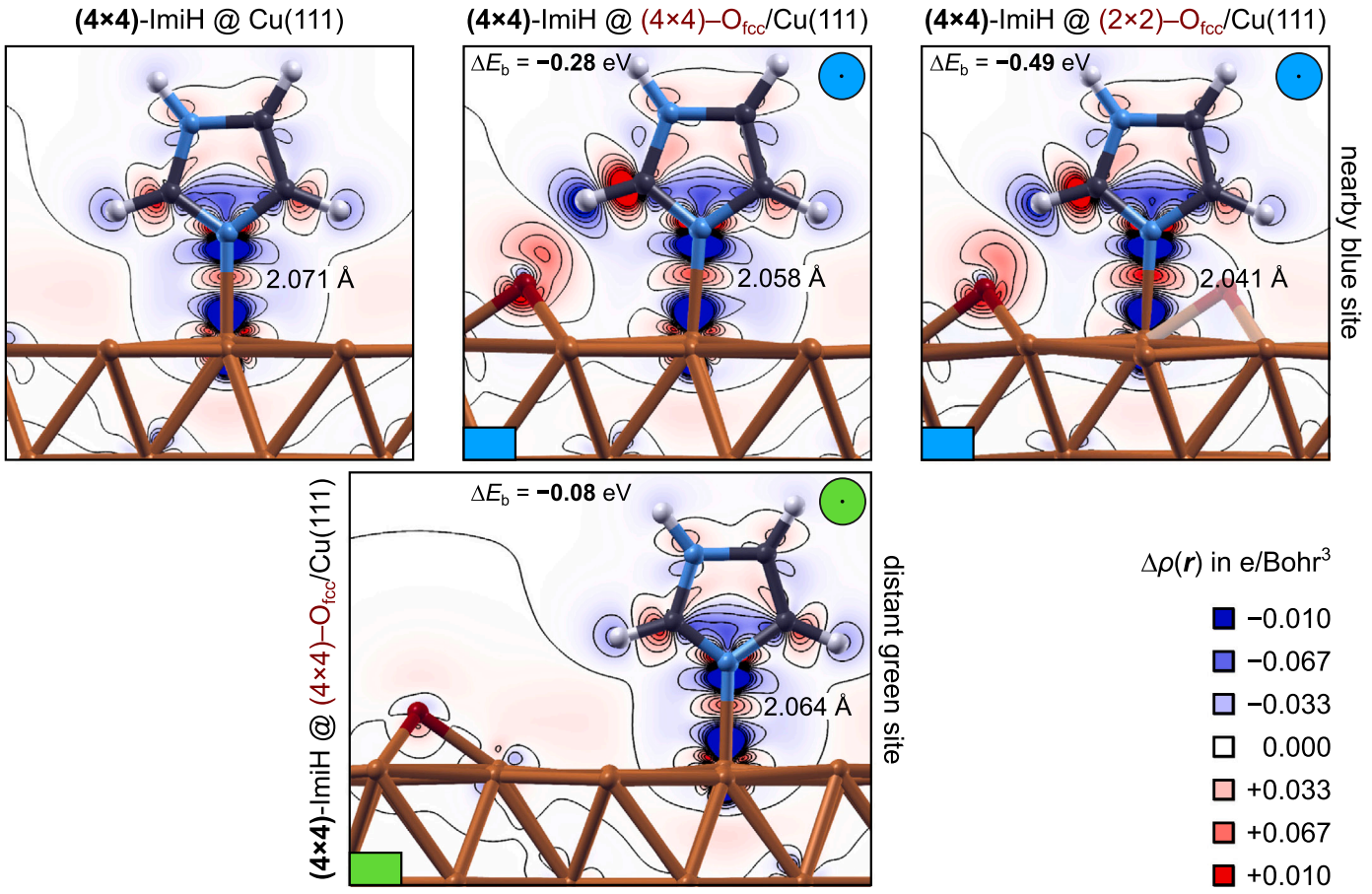

Fig. 13. Similar to Fig. 12, but here different $O_{(ads)}$ coverages are considered. From left to right: bare Cu(111), O/Cu(111) with 1/16 ML of $O_{(ads)}$, and O/Cu(111) with 1/4 ML of $O_{(ads)}$. In the top row plots, imidazole is adsorbed at the nearby blue sites of O/Cu(111), whereas in the bottom row plot, it is adsorbed on the more distant green site. In all cases, the coverage of imidazole is 1/16 ML, i.e., one imidazole molecule per (4 × 4)–Cu(111) supercell. The ΔE_b values and the N–Cu bond lengths are also reported. Note that for the blue sites, the electron charge accumulation in the middle of the N–Cu bond increases, and the N–Cu bond length decreases as the coverage of $O_{(ads)}$ increases. In contrast, at the green site, this red charge accumulation lobe is very similar to the one on bare Cu(111), although the N–Cu bond is marginally shorter than on bare Cu(111).

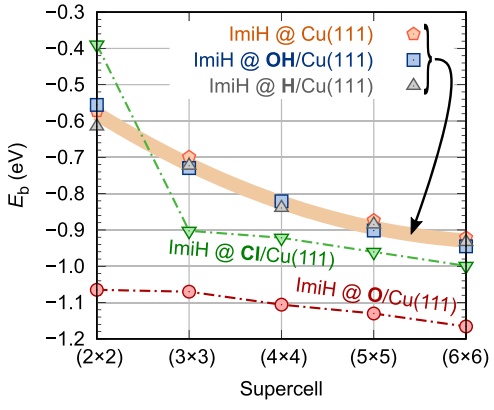

Fig. 14. The most exothermic binding energies (E_b) of imidazole on bare Cu (111) and Cu(111) precovered with the X species (X = H, O, OH, or Cl) as a function of the ($n \times n$) supercell size. This plot is based on data from Fig. 9, where structures with one imidazole and one X species per supercell are considered.

coverage of $X_{(ads)}$ (the top-view snapshots of these extra structures are also shown in Fig. 16). A similar analysis is also performed in Fig. S3 for imidazole adsorbed at nearest neighbor gray sites on H/Cu(111). The analysis shows that although imidazole can adsorb on gray sites, it is significantly destabilized there compared to other more distant sites or clean Cu(111). The destabilization increases with the $H_{(ads)}$ coverage for $\Theta > 1/3$ ML.

It is evident from Fig. 16 that ΔE_b depends linearly on the coverage of $X_{(ads)}$, i.e., the higher is the $X_{(ads)}$ coverage, the stronger is the ΔE_b effect, unless the coverage of $X_{(ads)}$ becomes so high as to hinder or even prevent the adsorption of imidazole due to steric reasons. For $Cl_{(ads)}$, this happens at $\Theta \gtrapprox 1/4$ ML (an example of $Cl_{(ads)}$ preventing the chemisorption of imidazole already at $\Theta = 1/4$ ML is shown for (2 × 2)–Cl/Cu (111) in Fig. 11a), whereas for $O_{(ads)}$ this happens somewhere in between 1/2 ML and 2/3 ML because our calculations indicate that imidazole cannot chemisorb at 2/3 ML of $O_{(ads)}$, as shown in Fig. S4. At this coverage, all surface Cu atoms are bonded to two O adatoms, hence all top sites are gray and, consequently, imidazole adsorbs with the N3 atom facing toward the fcc hollow site with the N–Cu distances of about 3.0 Å (Fig. S4). Surprisingly, imidazole adsorption is destabilized by only 0.1 eV with respect to clean Cu(111), i.e., $\Delta E_b = 0.10$ eV. Fig. 16 reveals that $O_{(ads)}$ and $Cl_{(ads)}$ stabilize adsorption of imidazole up to 0.77 and 0.35 eV, respectively. There is, however, a remarkable difference between $O_{(ads)}$ and $Cl_{(ads)}$. While Cl prefers to form the high-coverage 1/3 ML $(\sqrt{3} \times \sqrt{3})R30^\circ$–Cl/Cu(111) structure (Fig. S1b) [38,39] that, according to our results, blocks the chemisorption of imidazole, the 1/3 ML phase of $O_{(ads)}$ instead enhances the adsorption of imidazole

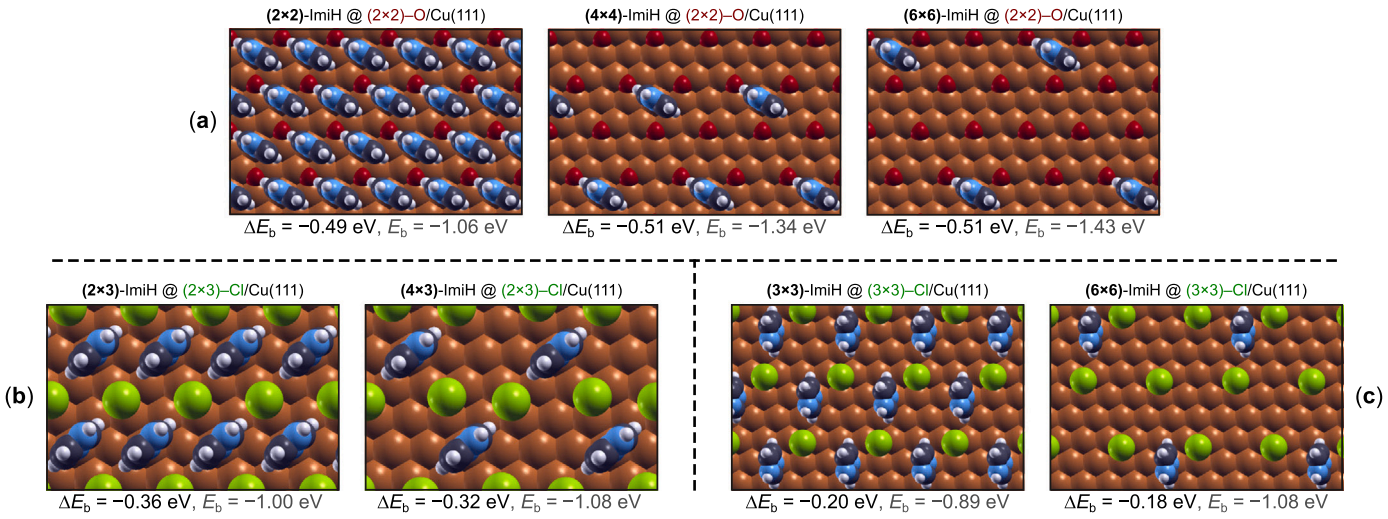

Fig. 15. Top-view snapshots of imidazole adsorbed on (a) (2 × 2)–O/Cu(111), (b) (2 × 3)–Cl/Cu(111), and (c) (3 × 3)–Cl/Cu(111). In (a) the coverage of imidazole reduces from 1/4 ML (left) to 1/36 ML (right), whereas considered coverages of imidazole in (b) are 1/6 and 1/12 ML and in (c) 1/9 and 1/36 ML. The corresponding ΔE_b and E_b values of imidazole are also stated. Note that for given $X_{(ads)}$ the ΔE_b values are to some extent invariant on the coverage of imidazole, but they depend on the coverage of $X_{(ads)}$ as evident from the comparison between (b) and (c).

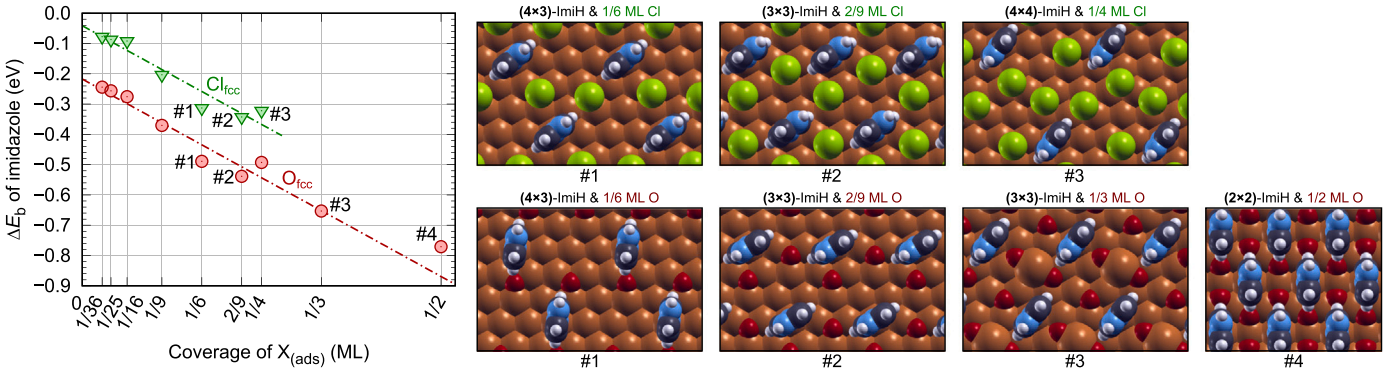

Fig. 16. Left: ΔE_b of imidazole on O/Cu(111) and Cl/Cu(111) as a function of the $O_{(ads)}$ and $Cl_{(ads)}$ coverage. At each $X_{(ads)}$ coverage, only the most stable identified imidazole structure is considered. Data are taken from Fig. 9, except datapoints labeled #1, #2, #3, and #4 correspond to the structures shown on the right. The #1 and #2 structures correspond to $2X_{(ads)}$ per (4 × 3) and (3 × 3) supercells, respectively, the $Cl_{(ads)}$ #3 structure corresponds to $4Cl_{(ads)}$ per (4 × 4) supercell (two Cl are adsorbed onto off-fcc and two Cl onto off-hcp sites, where the "off" prefix indicates that Cl is displaced from the hollow toward the bridge site), the $O_{(ads)}$ #3 structure corresponds to $3O_{(ads)}$ per (3 × 3) supercell with one O adsorbed onto hcp and two O onto fcc sites, whereas the $O_{(ads)}$ #4 structure consists of $2O_{(ads)}$ per (2 × 2) supercell with one O adsorbed onto hcp and the other one onto fcc sites. The ΔE_b values are always calculated with respect to the compatible ImiH @ X/Cu (111) vs. X/Cu(111) structures, where compatibility is achieved by removing imidazole from ImiH @ X/Cu(111) and relaxing the so obtained X/Cu(111) structure.

(note that the chemisorption phase diagram of O/Cu(111) is dominated by 1/4 ML and 1/3 ML phases, Fig. S1a).[7] The calculated low coverage adsorption energy of imidazole on clean Cu(111) is about −0.9 eV (Fig. 2), hence the optimum binding energy of imidazole on O/Cu(111) can be estimated to be about −1.6 eV, which is very similar to the adsorption energy of imidazole on coordinatively unsaturated Cu site of Cu_2O(111) [11,44–46].

As explained above by means of the $\Delta\rho(\mathbf{r})$ analysis (Fig. 12), the $O_{(ads)}$ strengthens the adsorption of imidazole due to the CH···O hydrogen bond and due to the $O_{(ads)}$ induced strengthening of the N–Cu bond (we refer to these two effects as the "local effects"). It is obvious that hydrogen bonding is a local effect because an H-bond between imidazole and $O_{(ads)}$ can only form if imidazole is adsorbed close enough to $O_{(ads)}$. Furthermore, the strengthening of the N–Cu bond also appears to be a local effect because the $\Delta\rho(\mathbf{r})$ analysis of Fig. 13 reveals that at the distant green site, this effect is not evident anymore. If these two effects were the only ones induced by $X_{(ads)}$, then it would be hard to understand why ΔE_b depends linearly on the $X_{(ads)}$ coverage. Moreover, notice from Fig. 9 that also distant sites are affected by the presence of $X_{(ads)}$, although the influence diminishes with the $X_{(ads)}$ coverage. Hence there should also be some non-local or global effect by which $X_{(ads)}$ affects the adsorption of imidazole. We will show in the next subsection that this global effect as well as the linear dependence of ΔE_b on the $X_{(ads)}$ coverage (cf. Fig. 16) is related to the $X_{(ads)}$ induced work function change, which also depends linearly on the coverage (cf. Fig. 3 and Eq. (20)). By extrapolating ΔE_b to zero coverage (Fig. 16), we can deduce the local effect of $X_{(ads)}$ on the binding of the nearby adsorbed imidazole (note that the zero coverage corresponds to a single imidazole adsorbed near a single $X_{(ads)}$ in the infinitely large supercell). The $O_{(ads)}$ induced ΔE_b of imidazole at zero coverage is −0.22 eV. This enhancement is too strong to be solely attributed to the CH···O hydrogen bond between imidazole and $O_{(ads)}$ because the strength of such H-bonds is estimated to be about 0.1 eV (see the Supplementary material of Ref. [47]). The remaining contribution thus comes from the $O_{(ads)}$ induced

[7] Otherwise, oxygen prefers thermodynamically to form either surface or bulk cuprous oxides [42,43], which should also be able to adsorb imidazole [44].

strengthening of the N–Cu bond.[8] For $Cl_{(ads)}$, the ΔE_b value at zero coverage is only −0.04 eV. Such a small magnitude can be attributed to a lack of hydrogen bonding.

3.6. Relation between work function and ΔE_b

The ΔE_b results presented in Fig. 9 show that $X_{(ads)}$ species affect the adsorption binding of imidazole not only on nearby sites but also on distant sites. However, the effect diminishes with the coverage of $X_{(ads)}$. The $\Delta\rho(\mathbf{r})$ plots of Fig. 13 also indicate that the $O_{(ads)}$ induced enhancement of the N–Cu bond diminishes as the coverage of $O_{(ads)}$ decreases, although in all these cases, imidazole is adsorbed at the blue site that is nearby $O_{(ads)}$. Last but not least, Fig. 16 reveals that the ΔE_b effect depends linearly on the coverage of $O_{(ads)}$ or $Cl_{(ads)}$. These observations indicate that some non-local effect affects the bonding of imidazole and diminishes as the coverage of $X_{(ads)}$ decreases. We propose that this effect is related to the work function or, more precisely, to the $X_{(ads)}$ induced change of the work function ($\Delta\Phi$), which depends linearly on the coverage of $X_{(ads)}$ (see Fig. 3). This proposition is not only supported by the observation that both $\Delta\Phi$ and ΔE_b depends linearly on the coverage of $X_{(ads)}$ (see Figs. 3 and 16) but, moreover, by the following evidence: $O_{(ads)}$ and $Cl_{(ads)}$ increase the work function (Fig. 3) and also strengthen the adsorption binding of imidazole ($\Delta E_b < 0$, Figs. 9 and 16), whereas $OH_{(ads)}$ decreases the work function and, consequently, diminishes the adsorption binding of imidazole (except for a few cases). $H_{(ads)}$ has a negligible effect on the work function and therefore affects ΔE_b insignificantly. The work function argument is made more quantitative by Fig. 17, which shows the dependence of ΔE_b on $\Delta\Phi$; in Fig. 17a all the sites from Fig. 9 are considered, however, to disentangle the local effects from the global work function effect, only the distant green sites are considered in Fig. 17b, whereas Fig. 17c instead considers only the stablest imidazole sites on O/Cu(111) and Cl/Cu(111), where the data from Fig. 16 are utilized. The linear correlation between ΔE_b and $\Delta\Phi$ is clearly evident, particularly in Figs. 17b and 17c. In contrast, the correlation in Fig. 17a is not as good because all the sites are considered therein, but only the nearby sites are affected by the additional stabilization due to local interactions between imidazole and $X_{(ads)}$, such as H-bonding (this is why the datapoints for the blue and yellow sites on O/Cu(111) appear below the regression line in Fig. 17a). It is worth noting that the regression line in Figs. 17b, which considers the distant green sites, passes very close to the $(\Delta\Phi, \Delta E_b) = (0, 0)$ point. The reason is that for the distant green sites, the local interactions between imidazole and $X_{(ads)}$ are missing, hence only the work function effect remains. According to the $\Delta\Phi$ hypothesis, the ΔE_b should be zero when $\Delta\Phi$ is zero, provided that local effects are missing, which is what happens precisely in Figs. 17b. Fig. 17 therefore provides a strong support for the work function hypothesis.

Why $\Delta\Phi$ of $X_{(ads)}$ affects ΔE_b of imidazole? One way to rationalize the relation between $\Delta\Phi$ and ΔE_b is by means of the electron charge-transfer parameter (ΔN) of the HSAB (Hard and Soft Acids and Bases) principle [48]. The rationalization is based on the premise that the adsorption binding energy is proportional to the charge transfer between the adsorbed molecule and the surface. This premise has been established for atomic and molecular adsorbates on transition metal surfaces [31,49,50]. Instead of the explicitly calculated charge of the adsorbed molecule, we utilize the ΔN parameter, firstly because it is physically easy to understand and secondly because it has been shown that it linearly correlates with the DFT calculated charge of adsorbed atoms [49,50] and molecules [31,49,51]. According to ΔN, the electron charge transfer between two fragments is proportional to their electronegativity difference and is opposed by the sum of their chemical hardnesses, i.e., electron charge transfer is promoted by a large difference in electronegativity and is opposed by a high chemical hardness. For the interaction between a molecule and a metal surface, the ΔN parameter is given by [49]:

$$\Delta N = \frac{\chi_{\text{surf}} - \chi_{\text{mol}}}{2(\eta_{\text{surf}} + \eta_{\text{mol}})} = \frac{\Phi - \chi_{\text{mol}}}{2\eta_{\text{mol}}}, \tag{23}$$

where χ and η stands for the Mulliken electronegativity and the chemical hardness, respectively, whereas the subscripts "surf" and "mol" stand for the surface and molecule, respectively. The electronegativity of the metal surface is given by its work function [49], while its chemical hardness is related to the inverse of the density of states at Fermi energy [52], which is an exceedingly small number for bulk metals, hence $\eta_{\text{surf}} = 0$ is an excellent approximation for metal surfaces that is utilized in Eq. (23).

For imidazole adsorbed on bare Cu(111), ΔN is given by:

$$\Delta N = \frac{\Phi_{\text{Cu(111)}} - \chi_{\text{ImiH}}}{2\eta_{\text{ImiH}}}, \tag{24}$$

whereas for imidazole adsorbed on X/Cu(111), it is given by:

$$\Delta N' = \frac{\Phi_{\text{X/Cu(111)}} - \chi_{\text{ImiH}}}{2\eta_{\text{ImiH}}}. \tag{25}$$

By utilizing the $E_b \propto -|\Delta N|$ premise[9] together with Eqs. (1)–(3), (24), and (25), the relation between ΔE_b and $\Delta\Phi$ is straightforwardly established, i.e.:

$$\begin{aligned} \Delta E_b = E_b' - E_b &\propto -(|\Delta N'| - |\Delta N|) \\ &\propto -\left(\frac{\Phi_{\text{X/Cu(111)}} - \chi_{\text{ImiH}}}{2\eta_{\text{ImiH}}} - \frac{\Phi_{\text{Cu(111)}} - \chi_{\text{ImiH}}}{2\eta_{\text{ImiH}}}\right) \\ &\propto -\frac{\Phi_{\text{X/Cu(111)}} - \Phi_{\text{Cu(111)}}}{2\eta_{\text{ImiH}}} \\ &\propto -\Delta\Phi, \end{aligned} \tag{26}$$

where

$$\Delta\Phi = \Phi_{\text{X/Cu(111)}} - \Phi_{\text{Cu(111)}}. \tag{27}$$

In the derivation of Eq. (26) the following relations were used:

$$\Phi_{\text{X/Cu(111)}} - \chi_{\text{ImiH}} > 0 \quad \text{and} \quad \Phi_{\text{Cu(111)}} - \chi_{\text{ImiH}} > 0. \tag{28}$$

Indeed, imidazole is less electronegative than Cu(111), i.e., the PBE calculated values are $\chi_{\text{ImiH}} = 4.32$ eV [51] and $\Phi_{\text{Cu(111)}} = 4.83$ eV [49]. X/Cu(111) surfaces are also more electronegative than imidazole (cf. Fig. 3), the only exception is OH_{fcc}/Cu(111) at 1/9 and 1/4 ML coverage. However, at such high coverage OH shifts to bridge site upon adsorption of imidazole and OH_{br}/Cu(111) is always more electronegative than imidazole because $\Delta\Phi_{OH_{br}} > -0.5$ eV (cf. Fig. 3), where −0.5 eV corresponds to $\chi_{\text{ImiH}} - \Phi_{\text{Cu(111)}}$.

The $\Delta E_b \propto -\Delta\Phi$ relation of Eq. (26) therefore provides a simple explanation of the trend observed in Fig. 17 and explains why $O_{(ads)}$ and $Cl_{(ads)}$ strengthen the bonding of imidazole on Cu(111), $H_{(ads)}$ has no effect, and $OH_{(ads)}$ diminishes the bonding of imidazole (except for a few cases).

[8] Although Fig. 13 suggests that this effect reduces with the $O_{(ads)}$ coverage, it seems that at zero coverage (corresponding to a single imidazole adsorbed near a single $O_{(ads)}$ in the infinitely large supercell), the effect does not vanish. A possible explanation is that the electronegative $O_{(ads)}$ makes the nearby Cu atoms slightly more electrophilic and thus more susceptible to binding with the electronegative N3 atom of imidazole.

[9] According to this premise, the higher the magnitude of the electron charge transfer between the adsorbate and the surface is, the more exothermic is the binding energy. This can be written as $E_b \propto -|\Delta N|$, which implies that only the magnitude and not the direction of the electron charge transfer matters.

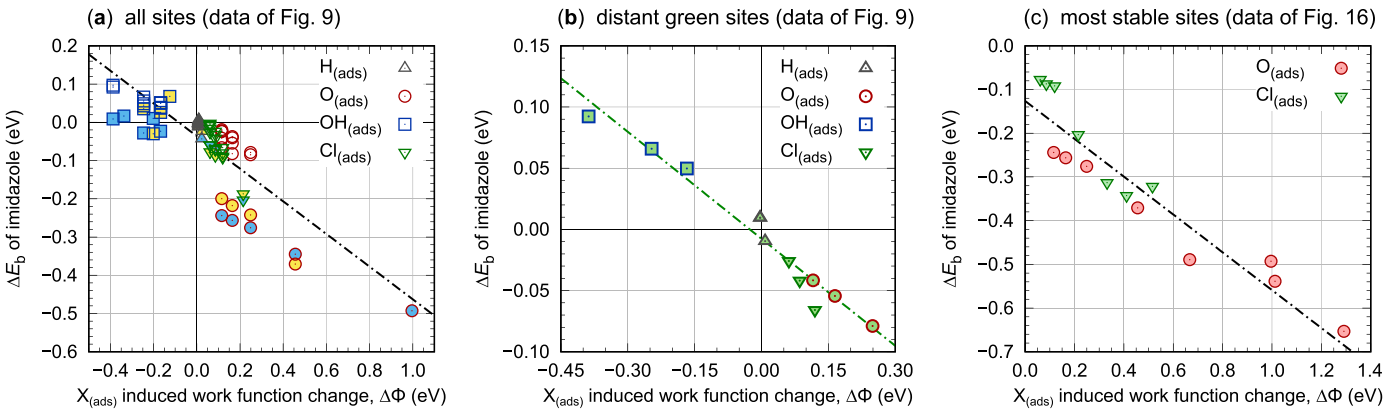

Fig. 17. ΔE_b of imidazole versus $X_{(ads)}$ induced work function change ($\Delta\Phi$). In (a) all the sites, in (b) the distant green sites, and in (c) the most stable sites at each coverage are considered. In (a) and (b) the ΔE_b values correspond to those in Fig. 9, whereas in (c) the data from Fig. 16 are used. In (a) the datapoints corresponding to the nearby blue and yellow sites are shown with blue and yellow background colors, whereas in (b) the datapoints are colored with a green background to indicate that they correspond to green sites.

3.7. Role of aqueous solvent

For obvious modeling reasons, the results presented in this manuscript correspond to *in vacuo* calculations. However, in the context of corrosion, the aqueous phase is relevant. To shed some light on how aqueous solvent affects the ΔE_b trends, we performed the calculations associated with Fig. 16 also in the implicit aqueous phase by using the soft-sphere-continuum-solvation method [53] as implemented in the `Environ` plugin [54,55] for Quantum ESPRESSO. Due to convergence problems, we could only perform single-point SCF calculations on the structures relaxed in a vacuum. The corresponding aqueous phase and *in vacuo* results are compared in Fig. S5 in the Supplementary material. These results reveal that the *in vacuo* ΔE_b trends are more or less preserved in the aqueous phase, although the ΔE_b magnitudes are diminished. This suggests that aqueous solvent screens, to some extent, the coadsorption effects.

4. Conclusions

The effect of chemisorbed H, O, OH, and Cl on the adsorption of imidazole on Cu(111) was scrutinized by means of systematic DFT calculations, where the role of the coverage, the type of $X_{(ads)}$ species, and the distance between imidazole and $X_{(ads)}$ were scrutinized. With respect to the lateral intersite distance between X adsorbed onto an fcc site and imidazole adsorbed on a top site, imidazole top sites can be classified into three regions: (i) Pauli repulsion region, consisting of the nearest neighbor top sites, where imidazole either cannot adsorb (for X = O, OH, and Cl) or is significantly hindered (for H); (ii) local region, consisting of the second and third nearest neighbor top sites, where H-bonds between $X_{(ads)}$ and imidazole are possible; and (iii) distant region consisting of sites that are further away and are therefore too far for hydrogen bonds to form.

The effect of $X_{(ads)}$ on adsorption of imidazole usually diminishes with the increasing imidazole–$X_{(ads)}$ distance and with the decreasing coverage of $X_{(ads)}$. Among the considered $X_{(ads)}$ species, $O_{(ads)}$ displays the strongest and the most stabilizing effect on the adsorption of imidazole (at high $O_{(ads)}$ coverage of about 1/2 ML, adsorbed imidazole can be stabilized by about 0.7 eV). $Cl_{(ads)}$ also stabilizes adsorption of imidazole but only up to about 0.3 eV, provided that the Cl coverage is not too high. In contrast, $H_{(ads)}$ has almost no effect, and $OH_{(ads)}$ usually diminishes the adsorption bonding of imidazole, except for the most stable cases where it displays a negligible effect. Among the four considered $X_{(ads)}$ species, the non-dissociatice adsorption of imidazole is, therefore, the most affected by $O_{(ads)}$ and $Cl_{(ads)}$. While both can enhance the adsorption bonding of imidazole, there is nevertheless a remarkable difference between the two. In particular, the critical $X_{(ads)}$ coverage where the chemisorption of imidazole is blocked is much lower for $Cl_{(ads)}$ than for $O_{(ads)}$, i.e., about 1/3 ML for $Cl_{(ads)}$ and about 2/3 ML for $O_{(ads)}$. While Cl prefers to form the high-coverage 1/3 ML $(\sqrt{3}\times\sqrt{3})R30^\circ$–Cl/Cu(111) structure that, according to our results, blocks the chemisorption of imidazole, oxygen is prone to form either 1/4 ML or 1/3 ML O/Cu(111) chemisorbed phases that both enhance the adsorption of imidazole. These considerations suggest that under real circumstances, the probability of enhancing the adsorption of imidazole is much higher for $O_{(ads)}$ than for $Cl_{(ads)}$.

We demonstrated that $X_{(ads)}$ species affect the adsorption of imidazole in three different ways: (i) via modification of the surface work function, which consequently affects the molecule–surface bonding. This is a global effect that depends linearly on the coverage of $X_{(ads)}$ and can either stabilize or destabilize the adsorbed azole molecule. (ii) Chemisorbed species, such as O and OH, can form stabilizing hydrogen bonds with adsorbed azole molecules. (iii) Chemisorbed O and Cl induce an enhancement of the N–Cu bond between adsorbed imidazole and the surface, provided that imidazole is adsorbed close enough to $X_{(ads)}$. This effect decreases with decreasing coverage of $X_{(ads)}$, but does not vanish at zero coverage, i.e., it persists even when imidazole is adsorbed near a single adsorbed $X_{(ads)}$. There is at least one other effect, which was not considered herein but will be covered in the subsequent publication [6]. It is the aftermath of the effect (ii), i.e., once the hydrogen bond between adsorbed azole and nearby $O_{(ads)}$ or $OH_{(ads)}$ is formed, the adsorbed molecule can be further stabilized by deprotonation that involves a proton shift from the molecule to chemisorbed O or OH.

CRediT authorship contribution statement

Matjaž Dlouhy: Investigation, Formal analysis, Writing – original draft, Writing – reviewing and editing, Visualization. **Anton Kokalj:** Conceptualization, Methodology, Investigation, Formal analysis, Writing – original draft, Writing – reviewing and editing, Visualization, Supervision, Project administration.

Declaration of Competing Interest

The authors declare that they have no known competing financial interests or personal relationships that could have appeared to influence the work reported in this paper.

Data availability

The raw/processed data required to reproduce these findings are

available in the open-source online data repository hosted at Mendeley Data, in particular at https://doi.org/10.17632/f7nh4vt8k5.1.

Acknowledgments

This work is a part of the M-Era.Net project entitled "COIN DESC: Corrosion inhibition and dealloying descriptors". The financial support of the project by MESS (Ministry of Education, Science, and Sport of the Republic of Slovenia, Grant No. C3330-17-500074) is acknowledged. This work has also been supported by the Slovenian Research Agency (Grant Nos. P2-0393 and PR-08976).

Appendix A. Supporting information

Supplementary data associated with this article can be found in the online version at doi:10.1016/j.corsci.2022.110443.

References

[1] J.O.'M. Bockris, A.K.N. Reddy, Modern Electrochemistry, second ed., Kluwer Academic/Plenum Publishers, New York, 2000.
[2] A. Kokalj, Molecular modeling of organic corrosion inhibitors: calculations, pitfalls, and conceptualization of molecule-surface bonding, Corros. Sci. 193 (2021), 109650, https://doi.org/10.1016/j.corsci.2021.109650.
[3] I.B. Obot, D.D. Macdonald, Z.M. Gasem, Density functional theory (DFT) as a powerful tool for designing new organic corrosion inhibitors. Part 1: an overview, Corros. Sci. 99 (2015) 1–30, https://doi.org/10.1016/j.corsci.2015.01.037.
[4] B. Hammer, J.K. Nørskov, Theoretical surface science and catalysis — calculations and concepts, Adv. Catal. 45 (2000) 71–129, https://doi.org/10.1016/S0360-0564(02)45013-4.
[5] Y.I. Kuznetsov, L.P. Kazansky, Physicochemical aspects of metal protection by azoles as corrosion inhibitors, Russ. Chem. Rev. 77 (2008) 219–232, https://doi.org/10.1016/S0013-4686(02)00811-3.
[6] A. Kokalj, M. Dlouhy, Dissociative adsorption of azoles on Cu(111) promoted by chemisorbed O and OH, Corros. Sci. (2022), https://doi.org/10.2139/ssrn.4122025.
[7] S.-W. Chen, Y.-J. Chen, Y.-H. Chen, G.-J. Chen, S.-H. Chan, J.-L. Lin, Adsorption and reaction pathways of 1H-1,2,3-triazole on Cu(100) and O/Cu(100), J. Phys. Chem. C 122 (48) (2018) 27412–27424, https://doi.org/10.1021/acs.jpcc.8b08007.
[8] J.-Y. Jhuang, S.-H. Lee, S.-W. Chen, Y.-H. Chen, Y.-J. Chen, J.-L. Lin, C.-H. Wang, Y.-W. Yang, Adsorption and reaction pathways of 1H-pyrazole on Cu(100) and O/Cu(100), J. Phys. Chem. C 122 (11) (2018) 6195–6208, https://doi.org/10.1021/acs.jpcc.8b00042.
[9] J.P. Perdew, K. Burke, M. Ernzerhof, Generalized gradient approximation made simple, Phys. Rev. Lett. 77 (18) (1996) 3865–3868, https://doi.org/10.1103/PhysRevLett.77.3865.
[10] S. Grimme, Semiempirical GGA-type density functional constructed with a long-range dispersion correction, J. Comput. Chem. 27 (15) (2006) 1787–1799, https://doi.org/10.1002/jcc.20495.
[11] D. Gustinčič, A. Kokalj, A DFT study of adsorption of imidazole, triazole, and tetrazole on oxidized copper surfaces: $Cu_2O(111)$ and $Cu_2O(111)$-w/o-Cu^{CUS}, Phys. Chem. Chem. Phys. 17 (2015) 28602–28615, https://doi.org/10.1039/C5CP03647J.
[12] E.R. McNellis, J. Meyer, K. Reuter, Azobenzene at coinage metal surfaces: Role of dispersive van der Waals interactions, Phys. Rev. B 80 (2009), 205414, https://doi.org/10.1103/PhysRevB.80.205414.
[13] K. Tonigold, A. Groß, Adsorption of small aromatic molecules on the (111) surfaces of noble metals: a density functional theory study with semiempirical corrections for dispersion effects, J. Chem. Phys. 132 (22) (2010), 224701, https://doi.org/10.1063/1.3439691.
[14] A. Kokalj, S. Peljhan, Density functional theory study of ATA, BTAH, and BTAOH as copper corrosion inhibitors: adsorption onto Cu(111) from gas phase, Langmuir 26 (18) (2010) 14582–14593, https://doi.org/10.1021/la1019789.
[15] D. Vanderbilt, Soft self-consistent pseudopotentials in a generalized eigenvalue formalism, Phys. Rev. B 41 (1990) 7892–7895, https://doi.org/10.1103/PhysRevB.41.7892.
[16] Ultrasoft pseudopotentials for H, C, N, O, Cl, and Cu atoms were taken from the Quantum ESPRESSO Pseudopotential Download Page at ⟨http://www.quantum-espresso.org/pseudopotentials⟩ (files: H.pbe-rrkjus.UPF, C.pbe-rrkjus.UPF, N.pbe-rrkjus.UPF, O.pbe-rrkjus.UPF, Cl.pbe-n-van.UPF, and Cu.pbe-d-rrkjus.UPF). (2021).
[17] P. Giannozzi, S. Baroni, N. Bonini, M. Calandra, R. Car, C. Cavazzoni, D. Ceresoli, G.L. Chiarotti, M. Cococcioni, I. Dabo, A. DalCorso, S. de Gironcoli, S. Fabris, G. Fratesi, R. Gebauer, U. Gerstmann, C. Gougoussis, A. Kokalj, M. Lazzeri, L. Martin-Samos, N. Marzari, F. Mauri, R. Mazzarello, S. Paolini, A. Pasquarello, L. Paulatto, C. Sbraccia, S. Scandolo, G. Sclauzero, A.P. Seitsonen, A. Smogunov, P. Umari, R.M. Wentzcovitch, Quantum ESPRESSO: a modular and open-source software project for quantum simulations of materials, J. Phys: Condens. Matter 21 (39) (2009), 395502, https://doi.org/10.1088/0953-8984/21/39/395502 code available from, ⟨http://www.quantum-espresso.org/⟩.
[18] P. Giannozzi, O. Andreussi, T. Brumme, O. Bunau, M.B. Nardelli, M. Calandra, R. Car, C. Cavazzoni, D. Ceresoli, M. Cococcioni, N. Colonna, I. Carnimeo, A. D. Corso, S. de Gironcoli, P. Delugas, R. DiStasio, A. Ferretti, A. Floris, G. Fratesi, G. Fugallo, R. Gebauer, U. Gerstmann, F. Giustino, T. Gorni, J. Jia, M. Kawamura, H.-Y. Ko, A. Kokalj, E. Küçükbenli, M. Lazzeri, M. Marsili, N. Marzari, F. Mauri, N. L. Nguyen, H.-V. Nguyen, A.O. de-la Roza, L. Paulatto, S. Poncé, D. Rocca, R. Sabatini, B. Santra, M. Schlipf, A.P. Seitsonen, A. Smogunov, I. Timrov, T. Thonhauser, P. Umari, N. Vast, X. Wu, S. Baroni, Advanced capabilities for materials modelling with Quantum ESPRESSO, J. Phys: Condens. Matter 29 (2017), 465901, https://doi.org/10.1088/1361-648X/aa8f79.
[19] A. Kokalj, PWTK: PWscf ToolKit, code available from ⟨http://pwtk.ijs.si/⟩ (2021).
[20] D.K. Kozlica, A. Kokalj, I. Milošev, Synergistic effect of 2-mercaptobenzimidazole and octylphosphonic acid as corrosion inhibitors for copper and aluminium – An electrochemical, XPS, FTIR and DFT study, Corros. Sci. 182 (2021), 109082, https://doi.org/10.1016/j.corsci.2020.109082.
[21] L. Bengtsson, Dipole correction for surface supercell calculations, Phys. Rev. B 59 (19) (1999) 12301–12304, https://doi.org/10.1103/PhysRevB.59.12301.
[22] H.J. Monkhorst, J.D. Pack, Special points for Brillouin-zone integrations, Phys. Rev. B 13 (12) (1976) 5188–5192, https://doi.org/10.1103/PhysRevB.13.5188.
[23] M. Methfessel, A.T. Paxton, High-precision sampling for Brillouin-zone integration in metals, Phys. Rev. B 40 (1989) 3616–3621, https://doi.org/10.1103/PhysRevB.40.3616.
[24] W. Tang, E. Sanville, G. Henkelman, A grid-based bader analysis algorithm without lattice bias, J. Phys: Condens. Matter 21 (8) (2009), 084204, https://doi.org/10.1088/0953-8984/21/8/084204.
[25] A. Arnaldsson, W. Tang, G. Henkelman, et al., Computer program for bader charge analysis, code avaialble from: http://theory.cm.utexas.edu/henkelman/code/bader/ (2019).
[26] P.E. Blöchl, Projector augmented-wave method, Phys. Rev. B 50 (24) (1994) 17953–17979, https://doi.org/10.1103/PhysRevB.50.17953.
[27] PAW potentials where obtained from a pseudopotenital library [55], https://dalcorso.github.io/pslibrary, version 1.0.0 (files: H.pbe-kjpaw_psl.1.0.0.UPF, C.pbe-n-kjpaw_psl.1.0.0.UPF, N.pbe-n-kjpaw_psl.1.0.0.UPF, O.pbe-n-kjpaw_psl.1.0.0.UPF, Cl.pbe-n-kjpaw_psl.1.0.0.UPF, and Cu.pbe-dn-kjpaw_psl.1.0.0.UPF). (2017).
[28] A. Kokalj, XCrySDen–a new program for displaying crystalline structures and electron densities, J. Mol. Graph. Model. 17 (1999) 176–179, https://doi.org/10.1016/S1093-3263(99)00028-5, code available from, ⟨http://www.xcrysden.org/⟩.
[29] T. Williams, C. Kelley, many others, Gnuplot 5.4, ⟨http://www.gnuplot.info/⟩ (2020).
[30] Inkscape Project, Inkscape, version 1.0.2, (2021). ⟨https://inkscape.org⟩.
[31] N. Kovačević, A. Kokalj, DFT study of interaction of azoles with Cu(111) and Al (111) surfaces: role of azole nitrogen atoms and dipole-dipole interactions, J. Phys. Chem. C 115 (49) (2011) 24189–24197, https://doi.org/10.1021/jp207076w.
[32] N. Kovačević, I. Milošev, A. Kokalj, The roles of mercapto, benzene, and methyl groups in the corrosion inhibition of imidazoles on copper: II. Inhibitor-copper bonding, Corros. Sci. 98 (2015) 457–470, https://doi.org/10.1016/j.corsci.2015.05.041.
[33] S. Sun, Y. Geng, L. Tian, S. Chen, Y. Yan, S. Hu, Density functional theory study of imidazole, benzimidazole and 2-mercaptobenzimidazole adsorption onto clean Cu (111) surface, Corros. Sci. 63 (2012) 140–147, https://doi.org/10.1016/j.corsci.2012.05.024.
[34] N. Kovačević, A. Kokalj, Analysis of molecular electronic structure of imidazole- and benzimidazole-based inhibitors: a simple recipe for qualitative estimation of chemical hardness, Corros. Sci. 53 (3) (2011) 909–921, https://doi.org/10.1016/j.corsci.2010.11.016.
[35] K. Cho, J. Kishimoto, T. Hashizume, H.W. Pickering, T. Sakurai, Adsorption and film growth of BTA on clean and oxygen adsorbed Cu(110) surfaces, Appl. Surf. Sci. 87/88 (1995) 380–385, https://doi.org/10.1016/0169-4332(94)00506-0.
[36] D.R. Lide. Ionic Radii in Crystals, eigthy five ed., CRC Press, Boca Raton, Florida USA, 2005, pp. 12/14–12/16 (Ch).
[37] S. Yang, X. Zhao, Z. Qi, Y.-H. Lu, G. Somorjai, P. Yang, A. Baskin, D. Prendergast, M. Salmeron, Chloride-assisted corrosion of copper and protection by benzotriazole, ACS Appl. Mater. Interfaces 14 (2022) 6093–6101, https://doi.org/10.1021/acsami.1c15808.
[38] P. Broekmann, M. Wilms, M. Kruft, C. Stuhlmann, K. Wandelt, In-situ STM investigation of specific anion adsorption on Cu(111), J. Electroanal. Chem. 467 (1) (1999) 307–324, https://doi.org/10.1016/S0022-0728(99)00048-0.
[39] S. Peljhan, A. Kokalj, Adsorption of chlorine on Cu(111): a density-functional theory study, J. Phys. Chem. C 113 (32) (2009) 14363–14376, https://doi.org/10.1021/jp902273k.
[40] D.K. Kozlica, J. Ekar, J. Kovač, I. Milošev, Roles of chloride ions in the formation of corrosion protective films on copper, J. Electrochem. Soc. 168 (3) (2021), 031504, https://doi.org/10.1149/1945-7111/abe34a.
[41] A. Kokalj, Corrosion inhibitors: physisorbed or chemisorbed? Corros. Sci. 196 (2022), 109939 https://doi.org/10.1016/j.corsci.2021.109939.
[42] A. Soon, M. Todorova, B. Delley, C. Stampfl, Oxygen adsorption and stability of surface oxides on Cu(111): a first-principles investigation, Phys. Rev. B 73 (2006), 165424, https://doi.org/10.1103/PhysRevB.73.165424.
[43] A. Soon, M. Todorova, B. Delley, C. Stampfl, Surface oxides of the oxygen-copper system: precursors to the bulk oxide phase? Surf. Sci. 601 (24) (2007) 5809–5813, https://doi.org/10.1016/j.susc.2007.06.062.

[44] D. Gustinčič, A. Kokalj, DFT study of azole corrosion inhibitors on Cu_2O model of oxidized copper surfaces: I. Molecule-surface and Cl-surface bonding, Metals 8 (5) (2018) 310, https://doi.org/10.3390/met8050310.
[45] D. Gustinčič, A. Kokalj, DFT study of azole corrosion inhibitors on Cu_2O model of oxidized copper surfaces: II. Lateral interactions and thermodynamic stability, Metals 8 (5) (2018) 311, https://doi.org/10.3390/met8050311.
[46] A. Kokalj, D. Gustinčič, M. Poberžnik, M. Lozinšek, New insights into adsorption bonding of imidazole: a viable C2–H bond cleavage on copper surfaces, Appl. Surf. Sci. 479 (2019) 463–468, https://doi.org/10.1016/j.apsusc.2018.12.246.
[47] L. Gašparič, M. Poberžnik, A. Kokalj, DFT study of hydrogen bonding between metal hydroxides and organic molecules containing N, O, S, and P heteroatoms: clusters vs. surfaces, Chem. Phys. 559 (2022), 111539, https://doi.org/10.1016/j.chemphys.2022.111539.
[48] R.G. Pearson, Absolute electronegativity and hardness: application to inorganic chemistry, Inorg. Chem. 27 (4) (1988) 734–740, https://doi.org/10.1021/ic00277a030.
[49] A. Kokalj, On the HSAB based estimate of charge transfer between adsorbates and metal surfaces, Chem. Phys. 393 (2012) 1–12, https://doi.org/10.1016/j.chemphys.2011.10.021.
[50] P. Crawford, P. Hu, Importance of electronegativity differences and surface structure in molecular dissociation reactions at transition metal surfaces, J. Phys. Chem. B 110 (49) (2006) 24929–24935, https://doi.org/10.1021/jp063472u.
[51] N. Kovačević, A. Kokalj, The relation between adsorption bonding and corrosion inhibition of azole molecules on copper, Corros. Sci. 73 (2013) 7–17, https://doi.org/10.1016/j.corsci.2013.03.016.
[52] W. Yang, R.G. Parr, Hardness, softness, and the fukui function in the electronic theory of metals and catalysis, Proc. Natl. Acad. Sc. USA 82 (20) (1985) 6723–6726, https://doi.org/10.1073/pnas.82.20.6723.
[53] G. Fisicaro, L. Genovese, O. Andreussi, S. Mandal, N.N. Nair, N. Marzari, S. Goedecker, Soft-sphere continuum solvation in electronic-structure calculations, J. Chem. Theory Comput. 13 (8) (2017) 3829–3845, https://doi.org/10.1021/acs.jctc.7b00375.
[54] O. Andreussi, I. Dabo, N. Marzari, Revised self-consistent continuum solvation in electronic-structure calculations, J. Phys. Chem. 136 (6) (2012), 064102, https://doi.org/10.1063/1.3676407.
[55] A. Dal Corso, Pseudopotentials periodic table: From H to Pu, Comp. Mater. Sci. 95 (2014) 337–350, https://doi.org/10.1016/j.commatsci.2014.1017 07.043.